Development 136, 965-973 (2009) doi:10.1242/dev.029868

Requirement for Sun1 in the expression of meiotic reproductive genes and piRNA

Ya-Hui Chi[1,2], Lily I. Cheng[3], Tim Myers[4], Jerrold M. Ward[3], Elizabeth Williams[3], Qin Su[4], Larry Faucette[3], Jing-Ya Wang[2] and Kuan-Teh Jeang[1,*]

The inner nuclear envelope (NE) proteins interact with the nuclear lamina and participate in the architectural compartmentalization of chromosomes. The association of NE proteins with DNA contributes to the spatial rearrangement of chromosomes and their gene expression. Sun1 is an inner nuclear membrane (INM) protein that locates to telomeres and anchors chromosome movement in the prophase of meiosis. Here, we have created *Sun1*$^{-/-}$ mice and have found that these mice are born and grow normally but are reproductively infertile. Detailed molecular analyses showed that *Sun1*$^{-/-}$ P14 testes are repressed for the expression of reproductive genes and have no detectable piRNA. These findings raise a heretofore unrecognized role of Sun1 in the selective gene expression of coding and non-coding RNAs needed for gametogenesis.

KEY WORDS: Sun1, Sad1, Unc84, Nuclear envelope, Gametogenesis, piRNA, Mouse

INTRODUCTION

The nuclear envelope (NE) sequesters chromosomes in the nucleus, separating them from the cytoplasm. In addition to providing anchoring sites for chromatin, the nuclear membrane is important for cellular metabolic activities. For example, the nuclear pore complex (NPC) supports the selective exchange of macromolecules between the nucleus and the cytoplasm (Schneider and Grosschedl, 2007), and the nuclear lamina can bind chromatin and regulate DNA replication and transcription (Ellis, 2006). Moreover, the loss of NE function has been linked to a variety of dystrophies, collectively termed 'nuclear envelopathies' (Schirmer et al., 2003). These diseases have phenotypes that include cardiac and skeletal myopathies, lipodystrophy, peripheral neuropathy and premature aging (Burke et al., 2001; Burke, 2001; Burke and Stewart, 2002; Espada et al., 2008; Worman and Courvalin, 2004).

How genes in the nucleus become accessible for processes such as transcription, replication or repair, and what factors are involved in these regulatory machineries are incompletely understood (Trinkle-Mulcahy and Lamond, 2007). One notion is that the NE proteins participate in modulating chromosome organization via direct contact or through indirect epigenetic events (Akhtar and Gasser, 2007; Shaklai et al., 2007). While transcriptionally active genes are frequently associated with the nuclear pore complex (Akhtar and Gasser, 2007), genome-wide studies of nuclear lamina-interacting loci have shown that the lamina-associated gene clusters are mostly repressed transcriptionally (Guelen et al., 2008; Pickersgill et al., 2006; Reddy et al., 2008). There is evidence that two LEM-domain-containing NE proteins, Emerin and Man1, play roles in tethering repressed genes to the nuclear periphery (Liu et al., 2003).

Sun1 is a mammalian INM protein that has a Sad1p-Unc84 (SUN) domain at its C terminus (Malone et al., 1999). The Sad1p protein in *Schizosaccharomyces pombe* is a constituent of the spindle pole body (SPB), which contacts the telomere complex (Chikashige et al., 2006). Disruption of the SPB abolishes its association with telomeres and obstructs meiotic recombination (Cooper et al., 1998). Conversely, the *Caenorhabditis elegans* SUN-domain protein Unc-84 is required for nuclear migration and anchorage (Lee et al., 2002). In mammalian cells, the N terminus of Sun1 targets the protein to the inner nuclear membrane (Chi et al., 2007), while the C terminus of the protein connects to cytoplasmic actin through a direct interaction with Nesprin (Crisp et al., 2006; Padmakumar et al., 2005). In somatic cells, human SUN1 has been described to be one of the early INM factors that associate with segregated daughter chromosomes in anaphase, participating in post-mitotic chromatin de-condensation by recruiting a membrane-associated histone acetyl transferase, hALP (Chi et al., 2007).

To gain additional physiological insights into the function(s) of Sun1, we created *Sun1*$^{-/-}$ mice. *Sun1*$^{-/-}$ mice are born and grow normally; however, they are reproductively sterile. Gametogenesis in these mice was halted at meiotic prophase I. An analysis of the *Sun1*$^{-/-}$ mice revealed a prevalent loss in the expression of reproductive genes and small non-coding piRNAs. Although it has been suggested that the sterility of *Sun1*$^{-/-}$ mice arose from the loss of the mechanical function of Sun1 at meiotic telomeres (Ding et al., 2007), our current findings support that failed expression of reproductive genes and piRNAs further explains *Sun1*$^{-/-}$ sterility.

MATERIALS AND METHODS

Construction of *Sun1* knockout mice

The *Sun1* knockout vector was constructed by cloning a 0.9 kb fragment containing exon 10, intron 10 and exon 11 of the mouse *Sun1* gene into vector pGEM-7 (Promega, Madison, WI, USA). *Neo* was positioned upstream of exon 10. A 3.0 kb DNA fragment upstream of exon 10 and a 3.4 kb fragment downstream of exon 11 were placed before the 5′ end of *Neo* and after the 3′ end of exon 11, respectively (Fig. 1A). The *HSV-TK* gene was placed at the 5′ end for negative selection. In addition, three *loxP* (locus of X-over of bacteriophage P1) sites were created at 5′ end of *Neo*, between

[1]Molecular Virology Section, Laboratory of Molecular Microbiology, National Institute of Allergy and Infectious Diseases, National Institutes of Health, Bethesda, MD 20892, USA. [2]Institute of Cellular and System Medicine, National Health Research Institutes, Zhunan 35053, Taiwan. [3]Infectious Disease Pathogenesis Section, Comparative Medicine Branch, Division of Intramural Research, National Institute of Allergy and Infectious Diseases, National Institutes of Health, Bethesda, MD 20892, USA. [4]Microarray Research Facility, Genomic Technologies Section, Institute of Allergy and Infectious Diseases, National Institutes of Health, Bethesda, MD 20892, USA.

*Author for correspondence (e-mail: kj7e@nih.gov)

Accepted 16 January 2009

Neo and exon 10, and at 3′ end of exon 11, respectively (Fig. 1A). *Sun1* knockout mice were generated by the Mouse Genome Engineering Facility at the University of Nebraska. In brief, the *Sun1* target vector was introduced into embryonic stem (ES) cells by electroporation and doubly selected using G418 and ganciclovir. Surviving clones were confirmed by polymerase chain reaction (PCR). Heterozygous ES cells were injected into C57BL/6J blastocysts. Mosaic founder animals were screened for germline transmission of the knockout genotype by breeding to C57BL/6J mice. F1 mice heterozygous for the knockout allele were mated to a Cre-expressing transgenic mouse [strain B6.FVB-Tg(EIIa-cre)C5379Lmgd/J, the Jackson Laboratory] resulting in the deletion of exon 10 and 11 of *Sun1* (Fig. 1A) in some offspring. Loss of exon 10-exon 11 was verified by PCR using primers: 5′-GGCAAGTGGATCTCTTGTGAATTCTTGAC-3′ and 5′-GTAGCACCCACCTTGGTGAGCTGGTAC-3′. Cre expression was confirmed using primers: 5′-GCGGTCTGGCAGTAAAAACTATC-3′ and 5′-GTGAAACAGCATTGCTGTCACTT-3′.

Preparation of anti-mouse Sun1 antibody

A DNA fragment corresponding to amino acids 701-913 of mouse Sun1 was cloned into the pET47b+ vector (Novagen, Gibbstown, NJ, USA) and expressed in *Escherichia coli* BL21(DE3) cells. The recombinant His-tagged mouse Sun1 (701-913) protein was purified using Ni-NTA agarose (Qiagen, Valencia, CA, USA), and the purified protein was used for rabbit immunization (Spring Valley Laboratories, Woodbine, MD, USA). Rabbit mouse Sun1 antiserum (αmusSun1-C) was further purified using protein A-agarose (Bio-Rad, Hercules, CA, USA).

Immunohistochemistry

Sections from paraffin-embedded fixed tissues were deparaffinized and rehydrated using xylene and ethanol. Antigen retrieval was achieved by placing the slides in boiling citrate buffer, pH 6.4 for 20 minutes. After cooling at room temperature for 20 minutes, slides were rinsed with ddH_2O and TBST (Tris-buffered saline with 0.1% Tween-20) successively. Endogenous peroxides were quenched by 3% H_2O_2 treatment for 10 minutes. To prevent non-specific binding, slides were blocked with background eraser (Biocare Medical, Concord, CA, USA) containing 10% goat serum for 5 minutes. Thereafter, primary (i.e. αmusSun1-C) antibody diluted with TBST was applied and slides were incubated in a humidified chamber for 1 hour. After rinsing with TBST, a biotinylated anti-rabbit IgG secondary antibody was added followed by incubation with a peroxidase-based Vectastain avidin-biotin complex (ABC, Vector Laboratories, Burlingame, CA, USA). Color was developed using DAB (3,3′-diaminobenzidine) substrate-chromogen. The nucleus was counterstained with Methyl Green.

Immunofluorescence and confocal microscopy

Cells or frozen sections were fixed with 4% paraformaldehyde for 30 minutes and permeabilized with 0.1% Triton X-100 in PBS for 5 minutes at room temperature. To avoid non-specific binding, cells were equilibrated with 1% BSA in PBS for 30 minutes. Antibodies against Sun1 (αmusSun1-C), γH2AX (Millipore, Billerica, MA, USA), Scp3 (Abcam, Cambridge, MA, USA), lamin B1 (Santa Cruz, Santa Cruz, CA, USA), Trf1 were added and slides were incubated for 1 hour at room temperature. Alexa-488-, Alexa-594- or Alexa-647-conjugated secondary antibodies were used for immunofluorescent detection. Fluorescent-conjugated secondary antibodies (Invitrogen, Carlsbad, CA, USA) were used for detection. Nuclei were stained with DAPI (Invitrogen). Cells on the coverslips were mounted on glass slides with antifade reagent (Invitrogen). Slides were monitored using a Leica TCS-NP/SP confocal microscope.

Microarray analysis

Total RNA was isolated from E14.5 mouse embryonic fibroblasts (MEFs) and whole testes of day 9, 14 or 28 mice using the RNeasy kit form Qiagen. cDNA was prepared by reverse transcription using Superscript II reverse transcriptase (Invitrogen) incorporated with Cy3- or Cy5-labeled dUTP. Thereafter, parental RNA was degraded by treating with 1 M NaOH at 70°C for 10 minutes; the reaction was neutralized by the addition of an equal volume of 1 M HCl. cDNA samples from paired (same parents) wild-type (Cy3-labeled) and $Sun1^{-/-}$ (Cy5-labeled) mice were mixed and hybridized to a 38 k, self-printed microarray (NCBI GEO accession number GPL6806). This array encompassed approximately 25,000 murine genes. Arrays were scanned by a GenePix 4000B fluorescent scanner (Molecular Devices, Sunnyvale, CA, USA). Three sets of arrays were compared for each type of tissue. Data were analyzed by mAdb (MicroArray DataBase) developed by CIT (Central for Information Technology, NIH) and IPA (Ingenuity pathways analysis, Ingenuity Systems) software.

Northern blotting

Northern blots for detecting miRNAs, Mili- or Miwi-associated piRNAs were performed according to published protocols (Aravin et al., 2006; Girard et al., 2006). In brief, 10 μg of total RNA were loaded per well. The oligodeoxynucleotide probes were for Mili-associated piRNAs on chromosomes 9 (5′-TCCCTAGGAGAAAATACTAGACCTAGAA-3′) and 17 (5′-TCCTTGTTAGTTCTCACTCGTCTTTTA-3′), for Miwi-associated piRNAs (piR-1, 5′-AAAGCTATCTGAGCACCTGTGTTCATGTCA-3′; piR-2, 5′-ACCAGCAGACACCGTCGTATGCATCACACa-3′; piR-3, 5′-ACCACTAAACATTTAGATGCCACTCTCA-3′), and for miR-16 (5′-GCCAATATTTACGTGCTGCTA-3′) and U6 snRNA (5′-GCAGGG-GCCATGCTAATCTTCTCTGTATCG-3′). The probes were radiolabeled with [α-^{32}P]-UTP using T7-RNA polymerase. After the reaction, the template DNA was degraded by DNase I and the probe was purified by gel filtration through a G-25 column (Millipore, Billerica, MA, USA). Hybridization using these probes was performed at 30°C in ULTRAhyb (Applied Biosystems, Austin, TX, USA) buffer for 24 hours. The membrane was washed three times with 2×SSC, 0.1% SDS solution at 30°C. Membranes were exposed to an IP plate, which was then scanned using a FLA-7000 imager (Fujifilm, Stamford, CT, USA).

RT-PCR of small RNAs

Total RNA from mouse testis was prepared, and small RNA (<200 nucleotides) was enriched using the *mir*Vana miRNA isolation kit (Applied Biosystems, Austin, TX, USA). The extracted total small RNAs were poly-A extended at their 3′ ends using poly(A) polymerase (Applied Biosystems). After annealing with a poly(T) adapter (5′-GCGAGCACAGAATTAAT-ACGACTCACTATAGGTTTTTTTTTTTVN-3′; V=A,C,G; N=A,T,C,G), RNA was reverse transcribed using Superscript II reverse transcriptase. PCR was performed using a universal reverse primer (5′-GCGAGCACAGA-ATTAATACGACT-3′) and a forward primer corresponding to individual piRNA or miR-16, respectively, as described above in the northern blot section. The RT-PCR products of small RNAs were analyzed by 15% denaturing urea-polyacrylamide gels. Primer sequences used for RT-PCR of Line-1 type A element (Line-1 A-F1, 5′-GAGTTTTGAGTCTGTATCC-3′; Line-1 A-R1, 5′-CTCTCCTTAGTTTCAGTGG-3′) were from Kuramochi-Miyagawa et al. (Kuramochi-Miyagawa et al., 2008).

RESULTS

Construction of *Sun1*$^{-/-}$ mice

Mouse Sun1 is an inner nuclear membrane protein with three nuclear transmembrane domains spanning amino acids 358 to 431 (Padmakumar et al., 2005). The N terminus of Sun1 is required for its inner nuclear membrane localization (Chi et al., 2007; Liu et al., 2007), while the SUN C terminus connects to the cytoskeleton through nesprin (Padmakumar et al., 2005). To investigate the physiological function of mammalian Sun1, we generated a *Sun1* knockout mouse by targeted deletion of exons 10 and 11 (amino acids 344 to 408) that correspond to the transmembrane domains. To guard against embryonic lethality of *Sun1* homozygous null animals, we created first a conditionally knocked out mouse. As illustrated in Fig. 1A, independent founder mice with three *loxP* sequences flanking a *Neo* (neomycin) gene, exon 10, and exon 11 were created; germ line transmission from founder to F1 offspring was confirmed by PCR (Fig. 1B, left panel). Next, to delete exons 10 and 11 from *Sun1*, we mated F1 animals to a strain of transgenic mouse from the Jackson Laboratory [strain B6.FVB-Tg(EIIa-cre)C5379Lmgd/J] that expresses an adenovirus *EIIa* promoter-driven Cre-expression

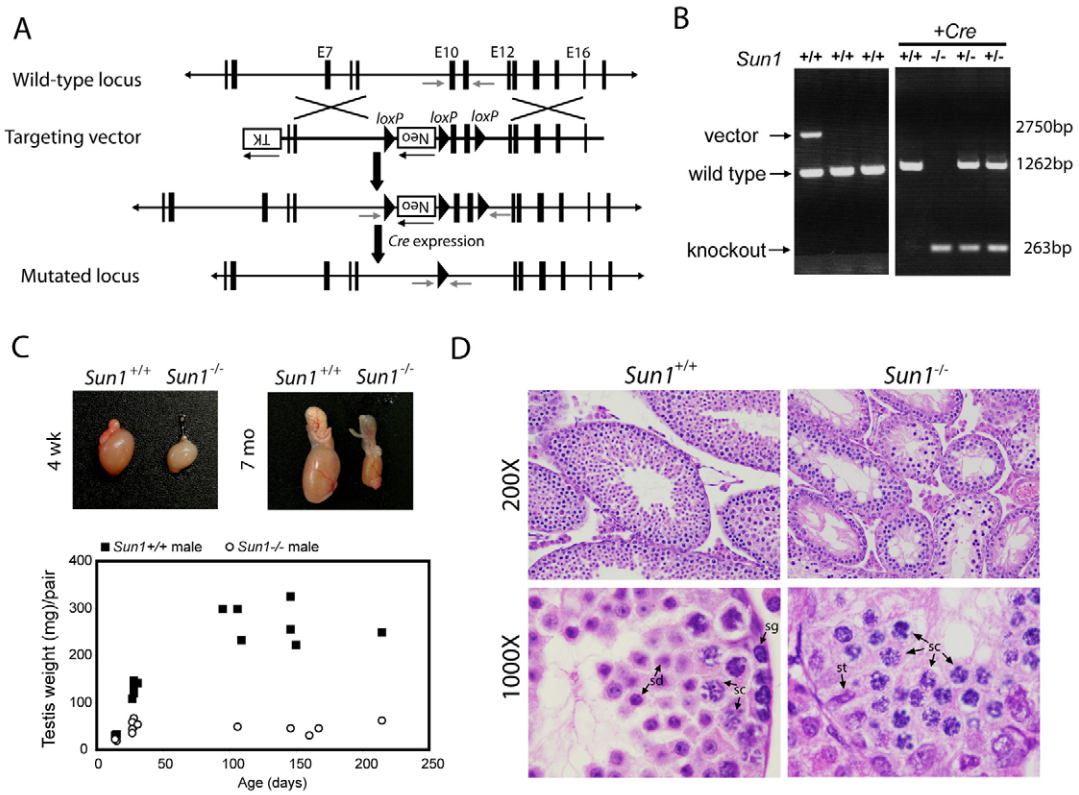

Fig. 1. Defective gametogenesis in *Sun1*$^{-/-}$ mice. (**A**) Schematic representation of the wild-type allele, the targeting vector and the mutated locus. The targeting vector contains the PGK-*Neo* gene (*Neo*) and the thymidine kinase gene (*TK*). Three *loxP* sites (denoted by black triangles) were placed at the 5′ end of *Neo*, between *Neo* and exon 10 (E10) and at the 3′ end of exon 11. *Sun1* was removed by crossing mice carrying the *Sun1* targeting vector with whole-body *Cre* transgenic mice. Gray arrows indicate the relative positions of primers used for genotyping by PCR. (**B**) PCR analysis of representative *Sun1* offspring from heterozygous matings. PCR of wild-type genomic DNA generates a 1262 bp fragment, whereas the targeting vector (left) generates a 2570 bp fragment. The sequence between the *loxP* sites was removed after *Cre* induction (right), and a 263 bp fragment was generated. (**C**) Comparison of testes from 4-week- and 7-month-old *Sun1*$^{+/+}$ and homologous mutant *Sun1*$^{-/-}$ mice. Testes from *Sun1*$^{-/-}$ mice are smaller in both cases. Clear weight differences were observed at about 4-weeks post birth. (**D**) Hematoxylin and Eosin (H&E)-stained sections (200× and 1000× magnifications) of testis from 4-week-old mice. In *Sun1*$^{+/+}$ testis, a clear progression of the first wave of spermatogenesis with differentiated spermatids (sd) was observed. No spermatid was found in the *Sun1*$^{-/-}$ mice. Instead, accumulation of zygotene-like spermatocytes was frequently detected in the *Sun1*$^{-/-}$ seminiferous tubules. sg, spermatogonia; st, sertoli cells; sc, spermatocyte; sd, spermatid.

vector (Fig. 1A). Cre-mediated removal of *loxP*-flanked exon 10 and exon 11 in F2 mice (*Sun1*$^{+/-}$) was confirmed by PCR (Fig. 1B, right panel). We then bred pairs of *Sun1*$^{+/-}$ mice and successfully generated *Sun1*$^{-/-}$ offspring.

Sun1$^{-/-}$ mice are reproductively sterile

Although *Sun1* is expressed ubiquitously in most mouse tissues (see Fig. S1A in the supplementary material) (Crisp et al., 2006), *Sun1*$^{-/-}$ mice were born grossly normal, and they grew to 7 months of age with body weights that were indistinguishable from those of wild-type siblings (see Fig. S1B in the supplementary material). However, when we paired *Sun1*$^{-/-}$ mice for mating, we discovered that the mice were infertile. This observation agrees with the results from a previously reported, albeit non-identical, *Sun1* knockout (KO) mouse (Ding et al., 2007). The reproductive sterility of our *Sun1*$^{-/-}$ mice was confirmed by multiple parings of 6-week-old male *Sun1*$^{+/+}$ with female *Sun1*$^{-/-}$ (four pairs) and male *Sun1*$^{-/-}$ with female *Sun1*$^{+/+}$ (four pairs) animals. None of the eight paired animals produced any pregnancy, supporting that both male and female *Sun1*$^{-/-}$ mice are infertile.

When the mice were sacrificed and necropsies were performed, we observed that adult *Sun1*$^{-/-}$ male gonads were significantly smaller than their counterpart wild-type organs (Fig. 1C). Large weight differences in the male gonads were seen when the animals were compared at 28 days post birth (Fig. 1C). Moreover, when compared to *Sun1*$^{+/+}$ mice, no sperm was seen in the epididymides of adult *Sun1*$^{-/-}$ testes (Fig. 1C; data not shown). In female *Sun1*$^{-/-}$ mice, no follicle was detected in the uterine tubes (see Fig. S1C in the supplementary material).

Four-week-old *Sun1*$^{+/+}$ testes had well-differentiated spermatocytes and spermatids (Fig. 1D); however, in *Sun1*$^{-/-}$ mice, the seminiferous tubules were blocked at the prophase of meiosis I (Fig. 1D). In the *Sun1*$^{-/-}$ mice, increased numbers of apoptotic cells were observed by TUNEL assay (see Fig. S1D in the supplementary material). Additionally, 4-week-old *Sun1*$^{-/-}$ ovaries contained no oocytes (see Fig. S1E in the supplementary material). The phenotype of our *Sun1* knockout mice is similar to that reported by Ding et al. (Ding et al., 2007). Unlike female mice whose oogenesis at meiosis I completes before birth, the first wave of spermatogenesis initiates 2 days postnatal. To further characterize

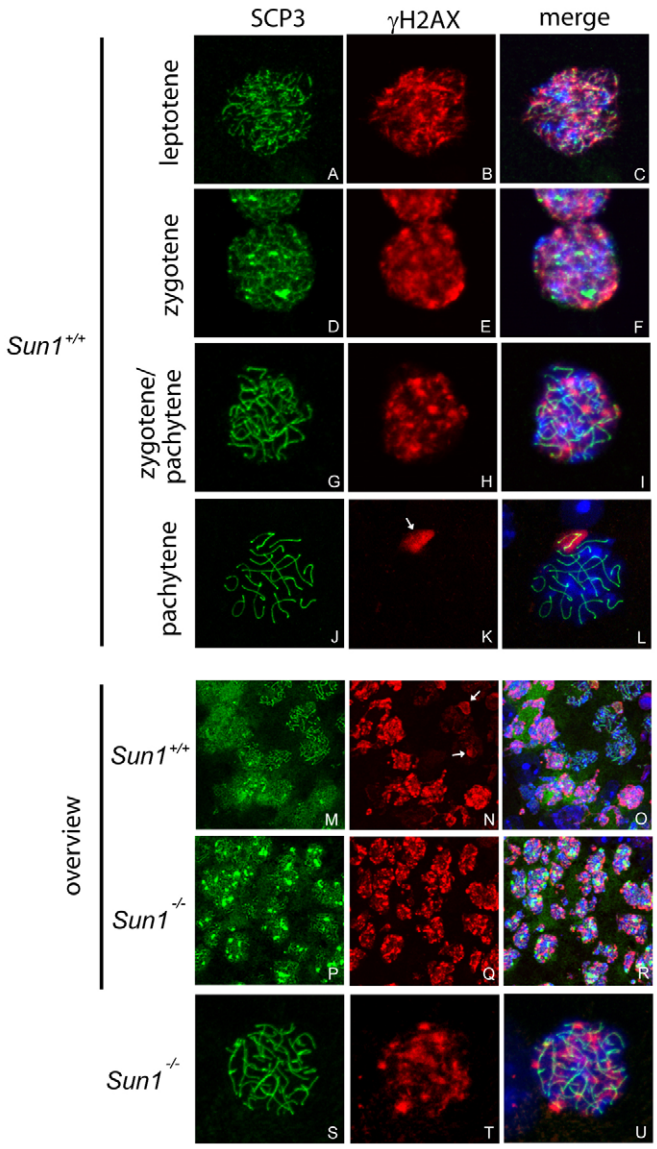

Fig. 2. Comparison of γH2AX staining in *Sun1*$^{+/+}$ versus *Sun1*$^{-/-}$ mice. Distribution of γH2AX (red, Alexa-594) in *Sun1*$^{+/+}$ (**A-O**) and *Sun1*$^{-/-}$ (**P-U**) testes at meiosis prophase I using spermatocyte spread (A-L,S-U) or cryosection (M-R). SCP3 (green, Alexa-488) staining denotes the stage of meiosis. A-L show single wild-type cells stained with γH2AX and SCP3. Overviews of testis cells (cryosections) in *Sun1*$^{+/+}$ (M-O) and *Sun1*$^{-/-}$ (P-R) are shown. A massive accumulation of γH2AX-stained cells was observed in *Sun1*$^{-/-}$ (P-R) but not in *Sun1*$^{+/+}$ (M-O) mice. In *Sun1*$^{+/+}$ leptotene spermatocytes, γH2AX was distributed all over the chromosome (panels 1-3). From zygotene to pachytene, γH2AX staining decreased gradually, and finally was restricted to the gonosomal chromatin in late zygotene/early pachytene spermatocytes (G-L). By contrast, *Sun1*$^{-/-}$ cells (spermatocyte spread) showed a general γH2AX staining pattern, similar to zygotene spermatocytes (P-U). Arrows in K and N denote the XY body.

which stage of meiosis was affected by *Sun1* depletion, we focused our analysis on postnatal male, rather than prenatal female, mice due to their easier experimental accessibility.

To characterize the gametogenesis defect, we used SCP3 (also called SYCP3) as an indicator for synaptonemal complex (SC) formation, and phosphorylation of histone H2A at Ser139 (i.e. γH2AX) as a marker for synapsis (Viera et al., 2004). SCP3 is a part of the lateral element of SC, a meiosis-specific protein structure that forms between two homologous chromosomes during meiosis and is essential for synapsis of homologous chromosomes (Zickler, 2006). Accumulation of γH2AX is an early response to induced double-strand breaks (DSBs), such as those seen in meiotic recombination. In the budding yeast and in the mouse, the initiation of synapsis is dependent on the occurrence of DSBs during leptotene and zygotene (Viera et al., 2004). During normal meiotic progression, SCP3 and γH2AX first appear diffusely in the leptotene stage of spermatocytes (Fig. 2A-C). As meiosis progresses to the zygotene stage, SCP3 forms a line-shaped structure, and γH2AX configures into discrete loci (Fig. 2D-F). In late zygotene and pachytene, γH2AX staining becomes restricted to the sex (XY) body, and prominent synapsis marked by SCP3 was observed [Fig. 2G-L, indicated by arrow) (Hamer et al., 2003; Sciurano et al., 2007). Intriguingly, although wild-type cells showed above expected progression in SCP3 and γH2AX staining (Fig. 2M-O), the distribution of γH2AX in *Sun1*$^{-/-}$ cells failed at the step of congression to the XY body (Fig. 2P-U). Thus, γH2AX in *Sun1*$^{-/-}$ cells remained multiply retained on various chromosomes (Fig. 2P-U), indicating that meiotic chromosome synapsis is impaired in *Sun1*-depleted cells.

Sun1 localization during spermatogenesis

To further investigate the role of Sun1 in gonad maturation, we generated an antibody (αmusSun1-C) to mouse Sun1. As shown in Fig. 3A, αmusSun1-C stained the nuclear envelope of mouse embryonic fibroblasts (MEFs), consistent with previous Sun1 localization studies (Chi et al., 2007; Padmakumar et al., 2005). Using αmusSun1-C, we performed immunohistochemical staining of mouse testes (Fig. 3B, part a), using Davidson's fixative with paraffin-embedding to preserve the organization of the tissue and the morphology of the cells. Employing Methyl Green to counterstain the nuclei, Sun1 was localized in progressively dividing meiotic cells (Fig. 3B, part a) and was found initially at the nuclear periphery in spermatogonia (Fig. 3B, part b). As the cells entered meiotic prophase I, the chromosomes condensed and Sun1 concentrated at the chromosome ends (Fig. 3B, parts c-f). Using a telomere marker, Trf1 (Scherthan et al., 2000), Sun1 stained coincidently, although did not completely overlap, with Trf1 at the telomeres; moreover, Sun1 was also associated with the nuclear membrane, as revealed by lamin B1 staining (Fig. 3C). By the second stage of meiosis when haploid chromatids were produced, Sun1 reappeared at the nuclear periphery (Fig. 3B, part g). As the spermatids elongated, an acrosome-acroplaxome-manchette complex formed to shape the chromatid head for packaging chromatin (Kierszenbaum and Tres, 2004). At this juncture, Sun1 located to the acrosome-like structure (Fig. 3B, part h). Subsequently, Sun1 staining was extinguished in spermatozoa (Fig. 3B, part i). These localization changes are compatible with dynamic roles for Sun1 in gamete production.

Prevalently changed meiotic gene expression in *Sun1*$^{-/-}$ versus control testes

The spatial organization of chromosomes in the nucleus can influence gene expression (Kumaran et al., 2008; Marshall, 2007; Stewart et al., 2007). Evidence suggests that a Sun1-telomere interaction tethers the chromosomes to the nuclear periphery, compartmentalizing DNA during the various stages of meiosis (Fig. 3). We wondered next how the depletion of Sun1 in *Sun1*$^{-/-}$ animals might impact meiotic gene expression.

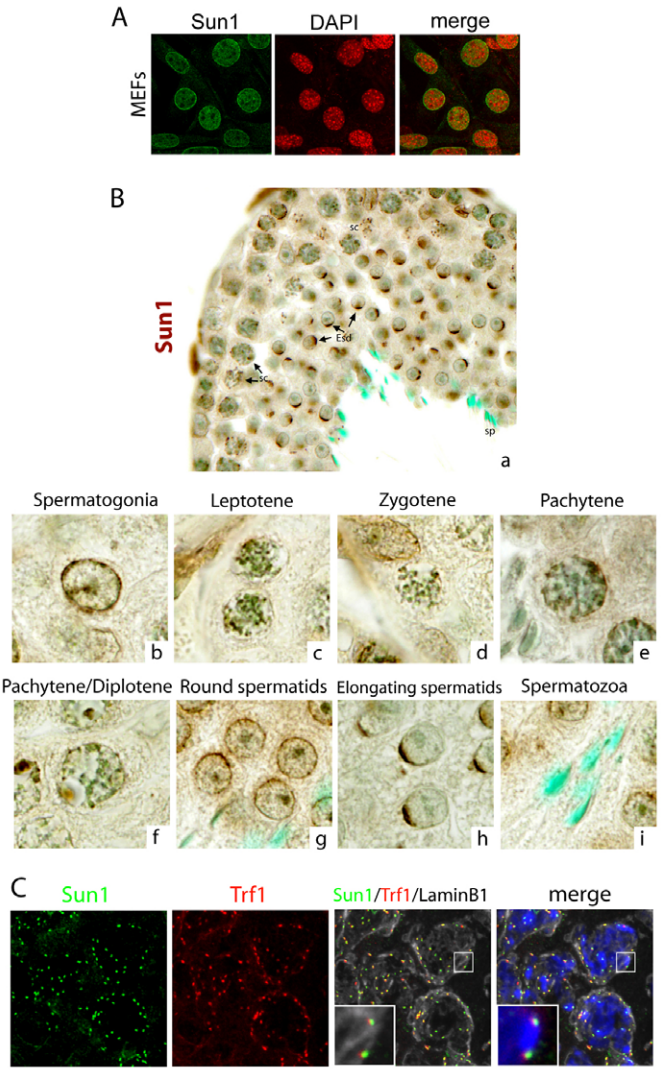

Fig. 3. Localization of Sun1 in the wild-type testis. (**A**) Immunofluorescent staining of Sun1 in mouse embryonic fibroblasts (MEFs) using αmusSun1-C. A clear nuclear envelope localization of Sun1 (green, Alexa-488) was seen. DNA stained by DAPI is in red. (**B**) Localization of Sun1 in the wild-type adult testis (Davidson's fixed, paraffin-embedded tissue section), as detected by immunohistochemistry. Sun1 is stained brown, and the nuclei were counterstained with Methyl Green (green). Part a shows an overall view of Sun1 staining in seminiferous tubule. Sun1 was localized to the nuclear periphery in spermatogonia (b) and round spermatids (g), showed punctate staining at chromosome ends in prophase I (c-f), and decorated an acrosome-like structure in elongated spermatids (h). Sun1 staining was not seen in spermatozoa (i). (**C**) Immunofluorescent staining of a frozen testis section (28-day-old) by αmusSun1-C (green, Alexa-488), anti-Trf1 (red, Alexa-594) and anti-lamin B1 (gray, Alexa-633) antibodies. Nuclei are labeled by DAPI (blue). Insets show higher-magnification images of the framed sections. sc, spermatocyte; sp, spermatozoan; Esd, elongated spermatid.

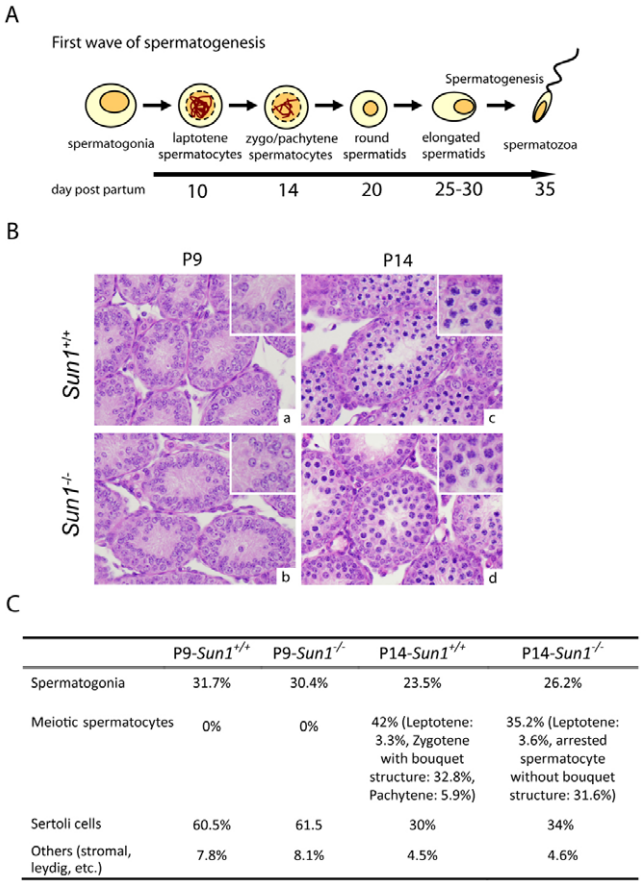

C

	P9-*Sun1*$^{+/+}$	P9-*Sun1*$^{-/-}$	P14-*Sun1*$^{+/+}$	P14-*Sun1*$^{-/-}$
Spermatogonia	31.7%	30.4%	23.5%	26.2%
Meiotic spermatocytes	0%	0%	42% (Leptotene: 3.3%, Zygotene with bouquet structure: 32.8%, Pachytene: 5.9%)	35.2% (Leptotene: 3.6%, arrested spermatocyte without bouquet structure: 31.6%)
Sertoli cells	60.5%	61.5	30%	34%
Others (stromal, leydig, etc.)	7.8%	8.1%	4.5%	4.6%

Fig. 4. Histology of testes from *Sun1*$^{+/+}$ and *Sun1*$^{-/-}$ mice during the first wave of spermatogenesis. (**A**) A schematic time line for the first wave of mouse spermatogenesis. (**B**) H&E stainings of testes from 9- and 14-day-old *Sun1*$^{+/+}$ and *Sun1*$^{-/-}$ mice are shown. Insets show higher-magnification images of the tissues. In P9 testes (a,b), no significant morphological difference was observed between *Sun1*$^{+/+}$ and *Sun1*$^{-/-}$ mice. In P14 mice, although the distribution of spermatogonia/sertoli cells and meiotic prophase I spermatocytes are similar (quantified in C) in the wild-type and *Sun1*$^{-/-}$ testes, wild type mostly showed clear 'bouquet' structures (c) while *Sun1*$^{-/-}$ cells did not (d). Cell stages later than pachytene were not observed in either P9 or P14 testes. (**C**) Cell compositions in P9 and P14 *Sun1*$^{+/+}$ and *Sun1*$^{-/-}$ testes. Two thousand cells were counted in each set.

In postnatal mice, the first wave of spermatogenesis transpires stepwise within the testis (Fig. 4A) (Goetz et al., 1984). At defined times, new germ cell types populate the testis, and the more immature cells progress to mature cells until the entire spectrum of germ cells is generated (Fig. 4A). To investigate how Sun1 might affect gene transcription, we compared male *Sun1*$^{+/+}$ and *Sun1*$^{-/-}$ germ cells in the initial stages of mouse spermatogenesis by using cDNA microarrays. The cell composition of P9 and P14 testes was quantified (Fig. 4B,C) according to the cell morphologies described by Russell et al. (Russell et al., 1990) and Bellve et al. (Bellve et al., 1977). The morphological and spatial arrangements of cells in *Sun1*$^{+/+}$ and *Sun1*$^{-/-}$ P9 testes were not grossly different (Fig. 4B,C). However, although the composition of cells was similar (Fig. 4C), the wild-type mice showed a clear bouquet structure at P14 (Fig. 4B,C), while the counterpart chromosomal appearance in *Sun1*$^{-/-}$ P14 testis was amorphous (Fig. 4B, part d). The consequences of bouquet formation or no bouquet formation in *Sun1*$^{+/+}$ or *Sun1*$^{-/-}$ mice were assessed next by comparing the gene expression profiles of P9 and P14 testes.

Total RNAs were extracted from 9- (P9, before prophase I) and 14- (P14, zygotene/pachytene) day-old mouse testes (Fig. 4A,B) and were analyzed using a 38 k gene chip representing 25,000 known

Table 1. Summary of cDNA microarray analysis* of *Sun1*$^{-/-}$ versus *Sun1*$^{+/+}$ gene expression in P9, P14 testis and MEFs

Number of:	P9 testis	P14 testis	MEFs
Data points in array	38 k	38 k	38 k
Genes with reproducibly (*P*<0.05) detectable signals	10,043	9280	6414
Genes 2-fold upregulated (*P*<0.05)	222†	109†	643
Genes 2-fold downregulated (*P*<0.05)	373†	834†	323
Genes less than 2-fold changed (*P*<0.05)	9448	8337	5448

*A 38,000 gene chip representing 25,000 mouse known genes was used for microarray analysis (NCBI GEO accession number GPL6806). cDNA was prepared from three paired (*Sun1*$^{-/-}$ and *Sun1*$^{+/+}$, from the same parents) animals for each array. Gene expression level of *Sun1*$^{-/-}$ versus *Sun1*$^{+/+}$ was calculated, and a *t*-test was used for evaluating statistical significance. For example, in P9 testis, in the 38,000 gene spots analyzed, 10,043 signals were reproducibly detected from three independent preparations. Among the 10,043 genes, 222 were >2-fold enhanced and 373 genes were >2-fold decreased. Expression differences were not significantly changed for the rest of the 9448 points.

†The statistical difference in gene expression between P9 and P14 testes is *P*<0.05 (Chi-square test, 222 versus 373 compared with 109 versus 834).

mouse genes (NCBI GEO accession number GPL6806). cDNA expression from three pairs of *Sun1*$^{-/-}$ versus *Sun1*$^{+/+}$ animals was evaluated at each of the two time points. We also compared the expression profiles of *Sun1*$^{-/-}$ versus *Sun1*$^{+/+}$ mouse embryonic fibroblasts (MEFs). Not all 25,000 array points were detected in the samples; however, the reproducibly detectable signals (*P*<0.05, *t*-test) from three separate assays were collated. Overall, 10,043 (P9 testes), 9280 (P14 testes) and 6414 (MEFs) data points were captured (Table 1). Comparing the *Sun1*$^{-/-}$ versus *Sun1*$^{+/+}$ samples, the expression of control 'housekeeping' genes such as actin or Gapdh was unchanged, and as expected *Sun1* (i.e. Unc84A) was consistently low in the *Sun1*$^{-/-}$ cDNA arrays (see Table S1 in the supplementary material).

The expression profiles of P9 *Sun1*$^{-/-}$ and *Sun1*$^{+/+}$ mouse testes showed that 9448 cDNAs were essentially unchanged, and approximately an equal number of genes were either two fold up- (222 out of 10,043, 2.2%) or down- (373 out of 10,043, 3.7%) regulated [a ratio of 1:1.6 in up- versus down-regulated genes (Table 1)]. This pattern became significantly different at P14 when the first wave of spermatogenesis proceeded to a stage between zygotene and pachytene and when bouquet structures were observed in most of the wild-type (Fig. 4B, part c) but not the *Sun1*$^{-/-}$ (Fig. 4B, part d) testis cells. At P14, 1.2% (109 out of 9280) of genes were upregulated and 9.0% (834 out of 9280) of genes were downregulated [a ratio of 1:7.5 in up- versus down-regulated genes (Table 1)]. Conversely, in non-germ control cells (i.e. MEFs), we actually noted that more genes were upregulated than were downregulated in the *Sun1*$^{-/-}$ compared with the *Sun1*$^{+/+}$ sample [a ratio of 1:0.5 in up- versus down-regulated genes (compare 643 to 323; Table 1)]. Collectively, these numbers suggest that a loss of Sun1 results in selectively downregulated gene expression in P14 germ cells.

Because *Sun1*$^{-/-}$ mice are infertile, we considered next whether reproductive genes (ontology analyses were made with the mAdb software developed by CIT, NIH, USA) were specifically repressed in these animals. We detected microarray signals for 119 reproductive genes in P9, and 162 reproductive genes in P14 germ cells. Although *Sun1*$^{-/-}$ and *Sun1*$^{+/+}$ P9 samples expressed essentially the same reproductive genes, P14 cells showed a 1:29 ratio in up- versus down-regulated genes in *Sun1*$^{+/+}$ samples (see Table 2). Of note, several genes, such as *Gykl1*, *Acr*, *Spag6*, *Odf4* and *Piwil1*, were repressed more than 10-fold [i.e. $\log_2$(*Sun1*$^{-/-}$/*wt*)<–3.3] in P14 *Sun1*$^{-/-}$ compared with *Sun1*$^{+/+}$ testis (see Table S2 in the supplementary material).

Reduction in Mili- and Miwi-associated piRNA in *Sun1*$^{-/-}$ testis

In our cDNA microarrays, reduced expression of *Miwi* (i.e. Piwil1; see Table S2 in the supplementary material) was seen in the *Sun1*$^{-/-}$ samples. Miwi and Mili are murine Piwi gene family members whose expression is restricted to mouse germ cells (Deng and Lin, 2002; Kuramochi-Miyagawa et al., 2004); they have been implicated in stem cell renewal, RNA silencing and germ cell development (Hartig et al., 2007; Klattenhoff and Theurkauf, 2008; Seto et al., 2007). To confirm the microarray results, we employed a semi-quantitative RT-PCR assay to measure the expression of *Miwi* and other reproduction-relevant genes in P9, P14 and P28 testes (Fig. 5A). Indeed, a reduction in *Miwi*, *Mili* and *Mvh1*, but not *Mlh1*, was observed.

Mili expression is crucial for germ cell progression to spermatids (Deng and Lin, 2002). The reduced expression of *Mili* could create a block in meiosis at a stage prior to pachytene in *Sun1*$^{-/-}$ cells. Mvh1 and Mili function before the zygotene stage (Kuramochi-Miyagawa et al., 2004; Tanaka et al., 2000), and it is intriguing that these two factors were also repressed in *Sun1*$^{-/-}$ animals. We noted that not all meiotic factors were affected. For example, the synaptonemal complex protein Scp3, the expression of which is restricted in leptotene to diplotene spermatocytes (Di Carlo et al., 2000; Meuwissen et al., 1992), was unchanged (Fig. 5A). Thus, the collective results suggested that an absence of *Sun1* selectively reduced the expression of many, but not all, reproductive genes.

Mili and Miwi function in the biogenesis of a novel class of 24- to 29-nucleotide piRNAs that accumulate during meiosis (Aravin et al., 2006; Girard et al., 2006). In addition, Mili forms a complex with Mvh1 in germ cells (Kuramochi-Miyagawa et al., 2004). Above, we documented the reduced expression of *Mili* and *Mvh1* in *Sun1*$^{-/-}$ germ

Table 2. Number of genes more than 2-fold changed that are associated with reproduction

Number of:	P9 testis	P14 testis
Reproductive genes in microarray	452	452
Reproductive genes with reproducibly (*P*<0.05) detectable signals	119	162
Genes 2-fold upregulated (*P*<0.05)	2*	1*
Genes 2-fold downregulated (*P*<0.05)	0*	29*
Genes less than 2-fold changed (*P*<0.05)	117	132

*The statistical difference in reproduction-associated gene expression between P9 and P14 testes is *P*=0.0008 (Chi-square test, 2 versus 0 compared with 1 versus 29).

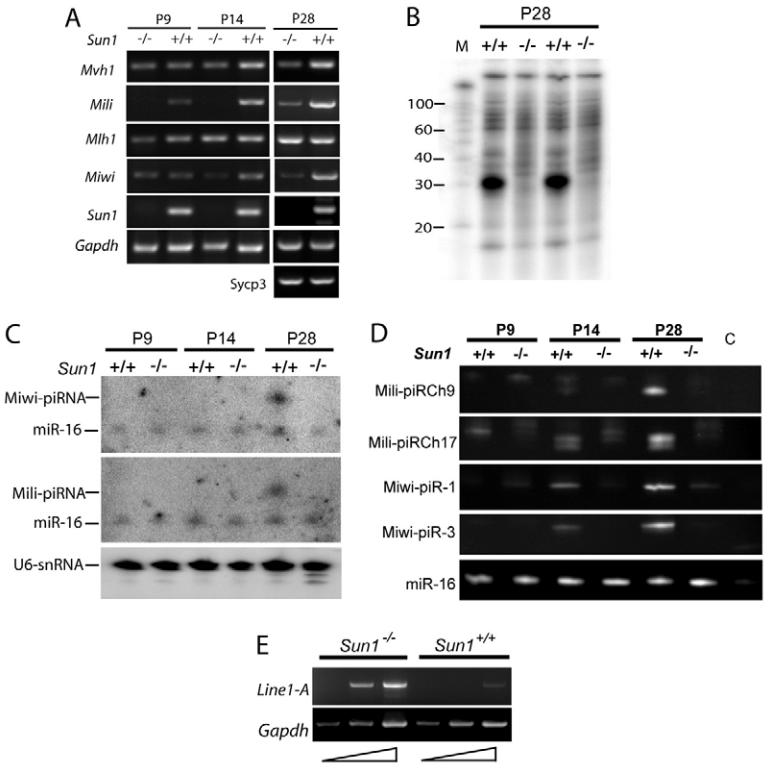

Fig. 5. Reduced Mili- and Miwi-associated piRNA expression in *Sun*$^{-/-}$ germ cells. (**A**) Semi-quantitative RT-PCR was used to validate the expression of spermatogenesis-related genes at P9, P14 and P28 testes. Gapdh was used for normalization. (**B**) Radioactive labeling of total RNAs isolated from 28-day-old mouse testis. *Sun1*$^{+/+}$ mice showed an abundant ~30-nucleotide small-RNA fraction while no detectable ~30-nucleotide small RNAs were seen in *Sun1*$^{-/-}$ mice. M, radio-labeled RNA ladder. (**C**) Northern blot hybridization for Mili- or Miwi-associated piRNAs. Ten micrograms of total mouse RNA were loaded in each lane. A mixture of probes against Mili-associated piRNAs from chromosome 9 and 17 or Miwi-associated piRNAs (piR-1, piR-2, piR-3) were used. A probe for microRNA miR-16 was hybridized simultaneously as a control. Blots were re-probed with a U6 antisense probe for comparison. (**D**) Semi-quantitative analysis of individual Mili- and Miwi-associated piRNA by RT-PCR. Expression of miR-16 is shown for normalization. C, control lane (no RNA was loaded in the reaction). (**E**) Semi-quantitative RT-PCR analysis of Line-1 type A element in *Sun1*$^{-/-}$ and *Sun1*$^{+/+}$ P14 testes. Gapdh expression was used as a control. Equal amounts of total RNA were used for RT-PCR cycles (25, 30 and 35 cycles from left to right, respectively).

cells (Fig. 5A). Because Mili and Miwi are necessary for piRNA production, their reduction could be independently confirmed by verifying the reduced expression of piRNA. To this end, we end-labeled total RNA with [γ-^{32}P]-ATP and assayed the abundance of small RNAs by denaturing gels. Notably, although wild-type mice harbored a surfeit of ~30-nucleotide piRNAs, these small RNA signals were not detected in 28-day-old *Sun1*$^{-/-}$ mice (Fig. 5B). Northern blotting using piRNA-specific probes (see Materials and methods) confirmed that the expected Mili- and Miwi-associated piRNAs were not seen in 28-day-old *Sun1*$^{-/-}$ testis (Fig. 5C). Moreover, we characterized the expression of several individual piRNAs using a highly sensitive RT-PCR assay. Thus, while Mili- and Miwi-associated piRNAs were seen in P14 *Sun1*$^{+/+}$ testis, little to no piRNAs were detected in P14 or P28 *Sun1*$^{-/-}$ testis by RT-PCR (Fig. 5D).

The silencing of transposable elements via de novo DNA methylation is required during gametogenesis, and the loss of *Mili* and *Miwi2* is associated with the activation of retrotransposons (Kuramochi-Miyagawa et al., 2008). To investigate whether the reduction in *Mili* and *Miwi* caused by *Sun1* depletion affected the expression of retrotransposons, we checked a representative Line-1 element using semi-quantitative RT-PCR (Kuramochi-Miyagawa et al., 2008). Indeed similar to findings from *Mili*$^{-/-}$ mice, the expression of type A Line-1 was de-repressed in two-week-old *Sun1*$^{-/-}$ testis (Fig. 5E).

DISCUSSION

The nuclear membrane and its associated proteins affect many cellular processes, including the spatial architecture of the DNA in the eukaryotic nucleus, which influences gene expression (Schneider and Grosschedl, 2007). We previously reported on the contribution of the inner nuclear membrane protein Sun1 to somatic cell mitosis and cell cycle progression (Chi et al., 2007). Others have presented findings that Sun1 provides a structural bridge that connects the nucleus to cytoplasmic actin and is involved in nuclear anchorage (Crisp et al., 2006; Padmakumar et al., 2005). Here, we have created a Sun1 knockout mouse, and have found, surprisingly, that the mouse is born somatically normal, and that the major in vivo developmental deficit in the *Sun1*$^{-/-}$ animal is reproductive infertility with failed gametogenesis.

Our experimental results agree with those of Ding et al. (Ding et al., 2007) that Sun1 locates to telomeres during the prophase of meiosis I (Fig. 3B,C). In lower eukaryotes that do not undergo meiotic reproduction, the published literature suggests that Sun1 behaves differently. For instance, the *S. pombe* Sun1 homolog Sad1 is a component of the spindle pole body (SPB) that serves as a microtubule organization center (Chikashige et al., 2006; Raff, 1999; Tomita and Cooper, 2006), and Matefin/SUN-1 of *C. elegans* has been reported to mediate the attachment of centrosomes to the nucleus (Penkner et al., 2007). In mammalian germ cells, Sun1 tethers telomeres to the nuclear periphery (Fig. 3) (Ding et al., 2007; Kierszenbaum and Tres, 2004). Our current study suggests that loss of this DNA compartmentalization reshapes the meiotic gene expression needed for normal gametogenesis (Table 2).

The report from Ding et al. (Ding et al., 2007) suggested that the association of Sun1 with telomeres is a prerequisite for efficient homolog paring and synapsis. At the initial stages of meiosis, paternal and maternal chromosomes converge and pair. Subsequently, homologous recombination could occur, and meiosis would then proceed to the next phase (Meier and Ahmed, 2001). Ding et al. (Ding et al., 2007) hypothesized that Sun1 functions in telomere clustering and bouquet formation, and that the bouquet structure facilitates the probability of encounter between chromosomes for recombination (Chikashige et al., 2006; Tomita and Cooper, 2006). Although this attractive hypothesis provides details on how Sun1 might contribute to bouquet formation and synapsis, it does not explain how these

events mechanistically influence downstream gametogenesis. Our data do not question the influence of Sun1 on bouquet formation, but they do suggest that loss of Sun1 further results in failed expression of selective reproductive genes and piRNAs, which would causally impact gametogenesis.

The cDNA microarray analyses revealed that in *Sun1*$^{-/-}$ versus *Sun1*$^{+/+}$ P9 testis, the ratio of up- versus down-regulated genes (1:1.6) was significantly different to the same ratio (1:7.5) in P14 testes (see Table 1). In *Sun1*$^{-/-}$ P9 testes, out of 119 reproductive genes with detectable signals, only two were different between *Sun1*$^{-/-}$ and *Sun1*$^{+/+}$ animals, whereas in P14 testes 30 reproductive genes were different, and 29 of these were repressed in *Sun1*$^{-/-}$ animals. How then does one link a loss of Sun1 to selectively changed meiotic gene expression? The answer is not known; however, recent experiments do show that siRNA-depletion of Sun1 interfered with the organization of the INM (inner nuclear membrane) constituents and the NPC (Chi et al., 2007; Liu et al., 2007). Transcriptionally active genes are frequently NPC associated (Taddei et al., 2006). Perhaps, a Sun1-depletion effect on the NPC could, in part, explain the selectively perturbed transcription in P14 *Sun1*$^{-/-}$ testes.

That Sun1 contributes to meiotic transcription is consistent with emerging data that some nuclear proteins previously touted only for their structural roles do significantly affect gene expression. For example, the cohesin protein whose function was attributed exclusively to connecting sister chromatids during mitosis and meiosis has recently been shown to serve a role in developmental gene regulation (Hallson et al., 2008; Misulovin et al., 2008). Likewise, the inner nuclear membrane protein Src1 was also revealed to regulate subtelomeric gene expression (Grund et al., 2008). Sun1 is a lamin A-binding protein (Crisp et al., 2006; Haque et al., 2006), and its currently invoked role in selective gene transcription may have implications for the competing models, the 'mechanical model' versus the 'gene expression model', that explain the pathogenesis of human laminopathies which arise from lamin A mutation (Wagner and Krohne, 2007). In the mechanical model, lamin A mutation weakens the cytoskeletal structure leading to disease pathology. By contrast, the gene expression model posits that lamin A mutation affects either directly or indirectly the expression of disease-associated genes that engender pathology. In considering the gametogenesis defect in *Sun1*$^{-/-}$ mice, one surmises that this could arise in two ways. First, *Sun1* depletion could abrogate proper chromosomal organization, interrupting meiosis and arresting gene expression. Second, *Sun1* depletion could selectively interfere with gene expression, whereby the loss of expression interrupts meiosis preventing proper chromosomal organization. Currently, the findings from *Sun1*$^{-/-}$ mice do not fully differentiate between whether Sun1 depletion impacts first chromosome organization or gene expression, or both simultaneously. Indeed, further dissection of the *Sun1* knockout mouse could potentially permit the delineation of which genes are involved in meiotic progression before and after bouquet formation.

Sun1 tethers lamin A through nesprin to cytoplasmic actin (Haque et al., 2006), and loss of Sun1 might be expected to show a similar mechano-structural weakness to that seen with a lamin A mutation. *Sun1*$^{-/-}$ mice, unlike *Lmna*$^{-/-}$ mice (Sullivan et al., 1999), however, do not exhibit a laminopathy. We speculate that the Sun1 function in *Sun1*$^{-/-}$ somatic cells may be redundantly constituted by the expression of other Sun domain proteins. However, based on our finding of selective repression of reproductive genes in *Sun1*$^{-/-}$ versus *Sun1*$^{+/+}$ testes, it may be worthwhile comparing in detail the gene expression patterns of relevant somatic tissues from *Lmna*$^{-/-}$ versus *Lmna*$^{+/+}$ mice for correlation with the development of pathology.

Another unanticipated observation to emerge from our work was the requirement for mouse Sun1 in the expression of Piwi-like proteins, Mili and Miwi. Mili and Miwi are expressed highly in testes and bind 24- to 29-nucleotide piRNAs. Both genes are required for male fertility as mice knocked out for either the *Mili* or the *Miwi* gene have degenerative male germ cells (Deng and Lin, 2002; Kuramochi-Miyagawa et al., 2004). In flies, piRNA mutations lead to the activation of retrotransposons. Mobilization of retrotransposition can create germline DNA damage and trigger cellular apoptotic responses (Brennecke et al., 2007). Indeed, piRNAs may serve ubiquitously to control chromatin organization, gene transcription, RNA stability or translation (Klattenhoff and Theurkauf, 2008). Consistent with these data, our results show that *Sun1*$^{-/-}$ germ cells do have higher retrotransposon expression (Fig. 5E). The detailed linkage between piRNA processing and Sun1 and the absence of piRNAs in *Sun1*$^{-/-}$ germ line cells needs further investigation, which could reveal a gamete-specific mechanism(s) that accounts for reproductive infertility.

We thank members of the Jeang laboratory for critical readings of this manuscript. This work was supported by in part NIAID/NIH intramural funds, the Intramural AIDS Targeted Anti-viral Program (IATAP), an NIAID contract to SoBran, and by intramural grants to Y.-H.C. from the National Health Research Institutes, Taiwan. Deposited in PMC for release after 12 months.

Supplementary material

Supplementary material for this article is available at http://dev.biologists.org/cgi/content/full/136/6/965/DC1

References

Akhtar, A. and Gasser, S. M. (2007). The nuclear envelope and transcriptional control. *Nat. Rev. Genet.* **8**, 507-517.

Aravin, A., Gaidatzis, D., Pfeffer, S., Lagos-Quintana, M., Landgraf, P., Iovino, N., Morris, P., Brownstein, M. J., Kuramochi-Miyagawa, S., Nakano, T. et al. (2006). A novel class of small RNAs bind to MILI protein in mouse testes. *Nature* **442**, 203-207.

Bellve, A. R., Cavicchia, J. C., Millette, C. F., O'Brien, D. A., Bhatnagar, Y. M. and Dym, M. (1977). Spermatogenic cells of the prepuberal mouse. Isolation and morphological characterization. *J. Cell Biol.* **74**, 68-85.

Brennecke, J., Aravin, A. A., Stark, A., Dus, M., Kellis, M., Sachidanandam, R. and Hannon, G. J. (2007). Discrete small RNA-generating loci as master regulators of transposon activity in Drosophila. *Cell* **128**, 1089-1103.

Burke, B. (2001). The nuclear envelope: filling in gaps. *Nat. Cell Biol.* **3,** E273-E274.

Burke, B. and Stewart, C. L. (2002). Life at the edge: the nuclear envelope and human disease. *Nat. Rev. Mol. Cell. Biol.* **3**, 575-585.

Burke, B., Mounkes, L. C. and Stewart, C. L. (2001). The nuclear envelope in muscular dystrophy and cardiovascular diseases. *Traffic* **2**, 675-683.

Chi, Y. H., Haller, K., Peloponese, J. M., Jr and Jeang, K. T. (2007). Histone acetyltransferase hALP and nuclear membrane protein hsSUN1 function in de-condensation of mitotic chromosomes. *J. Biol. Chem.* **282**, 27447-27458.

Chikashige, Y., Tsutsumi, C., Yamane, M., Okamasa, K., Haraguchi, T. and Hiraoka, Y. (2006). Meiotic proteins bqt1 and bqt2 tether telomeres to form the bouquet arrangement of chromosomes. *Cell* **125**, 59-69.

Cooper, J. P., Watanabe, Y. and Nurse, P. (1998). Fission yeast Taz1 protein is required for meiotic telomere clustering and recombination. *Nature* **392**, 828-831.

Crisp, M., Liu, Q., Roux, K., Rattner, J. B., Shanahan, C., Burke, B., Stahl, P. D. and Hodzic, D. (2006). Coupling of the nucleus and cytoplasm: role of the LINC complex. *J. Cell Biol.* **172**, 41-53.

Deng, W. and Lin, H. (2002). miwi, a murine homolog of piwi, encodes a cytoplasmic protein essential for spermatogenesis. *Dev. Cell* **2**, 819-830.

Di Carlo, A. D., Travia, G. and De Felici, M. (2000). The meiotic specific synaptonemal complex protein SCP3 is expressed by female and male primordial germ cells of the mouse embryo. *Int. J. Dev. Biol.* **44**, 241-244.

Ding, X., Xu, R., Yu, J., Xu, T., Zhuang, Y. and Han, M. (2007). SUN1 is required for telomere attachment to nuclear envelope and gametogenesis in mice. *Dev. Cell* **12**, 863-872.

Ellis, J. A. (2006). Emery-Dreifuss muscular dystrophy at the nuclear envelope: 10 years on. *Cell Mol. Life Sci.* **63**, 2702-2709.

Espada, J., Varela, I., Flores, I., Ugalde, A. P., Cadinanos, J., Pendas, A. M., Stewart, C. L., Tryggvason, K., Blasco, M. A., Freije, J. M. et al. (2008). Nuclear envelope defects cause stem cell dysfunction in premature-aging mice. *J. Cell Biol.* **181**, 9-13.

Girard, A., Sachidanandam, R., Hannon, G. J. and Carmell, M. A. (2006). A germline-specific class of small RNAs binds mammalian Piwi proteins. *Nature* **442**, 199-202.
Goetz, P., Chandley, A. C. and Speed, R. M. (1984). Morphological and temporal sequence of meiotic prophase development at puberty in the male mouse. *J. Cell Sci.* **65**, 249-263.
Grund, S. E., Fischer, T., Cabal, G. G., Antunez, O., Perez-Ortin, J. E. and Hurt, E. (2008). The inner nuclear membrane protein Src1 associates with subtelomeric genes and alters their regulated gene expression. *J. Cell Biol.* **182**, 897-910.
Guelen, L., Pagie, L., Brasset, E., Meuleman, W., Faza, M. B., Talhout, W., Eussen, B. H., de Klein, A., Wessels, L., de Laat, W. et al. (2008). Domain organization of human chromosomes revealed by mapping of nuclear lamina interactions. *Nature* **453**, 948-951.
Hallson, G., Syrzycka, M., Beck, S. A., Kennison, J. A., Dorsett, D., Page, S. L., Hunter, S. M., Keall, R., Warren, W. D., Brock, H. W. et al. (2008). The Drosophila cohesin subunit Rad21 is a trithorax group (trxG) protein. *Proc. Natl. Acad. Sci. USA* **105**, 12405-12410.
Hamer, G., Roepers-Gajadien, H. L., van Duyn-Goedhart, A., Gademan, I. S., Kal, H. B., van Buul, P. P. and de Rooij, D. G. (2003). DNA double-strand breaks and gamma-H2AX signaling in the testis. *Biol. Reprod.* **68**, 628-634.
Haque, F., Lloyd, D. J., Smallwood, D. T., Dent, C. L., Shanahan, C. M., Fry, A. M., Trembath, R. C. and Shackleton, S. (2006). SUN1 interacts with nuclear lamin A and cytoplasmic nesprins to provide a physical connection between the nuclear lamina and the cytoskeleton. *Mol. Cell. Biol.* **26**, 3738-3751.
Hartig, J. V., Tomari, Y. and Forstemann, K. (2007). piRNAs-the ancient hunters of genome invaders. *Genes Dev.* **21**, 1707-1713.
Kierszenbaum, A. L. and Tres, L. L. (2004). The acrosome-acroplaxome-manchette complex and the shaping of the spermatid head. *Arch. Histol. Cytol.* **67**, 271-284.
Klattenhoff, C. and Theurkauf, W. (2008). Biogenesis and germline functions of piRNAs. *Development* **135**, 3-9.
Kumaran, R. I., Thakar, R. and Spector, D. L. (2008). Chromatin dynamics and gene positioning. *Cell* **132**, 929-934.
Kuramochi-Miyagawa, S., Kimura, T., Ijiri, T. W., Isobe, T., Asada, N., Fujita, Y., Ikawa, M., Iwai, N., Okabe, M., Deng, W. et al. (2004). Mili, a mammalian member of piwi family gene, is essential for spermatogenesis. *Development* **131**, 839-849.
Kuramochi-Miyagawa, S., Watanabe, T., Gotoh, K., Totoki, Y., Toyoda, A., Ikawa, M., Asada, N., Kojima, K., Yamaguchi, Y., Ijiri, T. W. et al. (2008). DNA methylation of retrotransposon genes is regulated by Piwi family members MILI and MIWI2 in murine fetal testes. *Genes Dev.* **22**, 908-917.
Lee, K. K., Starr, D., Cohen, M., Liu, J., Han, M., Wilson, K. L. and Gruenbaum, Y. (2002). Lamin-dependent localization of UNC-84, a protein required for nuclear migration in Caenorhabditis elegans. *Mol. Biol. Cell* **13**, 892-901.
Liu, J., Lee, K. K., Segura-Totten, M., Neufeld, E., Wilson, K. L. and Gruenbaum, Y. (2003). MAN1 and emerin have overlapping function(s) essential for chromosome segregation and cell division in Caenorhabditis elegans. *Proc. Natl. Acad. Sci. USA* **100**, 4598-4603.
Liu, Q., Pante, N., Misteli, T., Elsagga, M., Crisp, M., Hodzic, D., Burke, B. and Roux, K. J. (2007). Functional association of Sun1 with nuclear pore complexes. *J. Cell Biol.* **178**, 785-798.
Malone, C. J., Fixsen, W. D., Horvitz, H. R. and Han, M. (1999). UNC-84 localizes to the nuclear envelope and is required for nuclear migration and anchoring during C. elegans development. *Development* **126**, 3171-3181.
Marshall, W. F. (2007). Centriole assembly: the origin of nine-ness. *Curr. Biol.* **17,** R1057-R1059.
Meier, B. and Ahmed, S. (2001). Checkpoints: chromosome pairing takes an unexpected twist. *Curr. Biol.* **11,** R865-R868.
Meuwissen, R. L., Offenberg, H. H., Dietrich, A. J., Riesewijk, A., van, I. M. and Heyting, C. (1992). A coiled-coil related protein specific for synapsed regions of meiotic prophase chromosomes. *EMBO J.* **11**, 5091-5100.
Misulovin, Z., Schwartz, Y. B., Li, X. Y., Kahn, T. G., Gause, M., MacArthur, S., Fay, J. C., Eisen, M. B., Pirrotta, V., Biggin, M. D. et al. (2008). Association of cohesin and Nipped-B with transcriptionally active regions of the Drosophila melanogaster genome. *Chromosoma* **117**, 89-102.
Padmakumar, V. C., Libotte, T., Lu, W., Zaim, H., Abraham, S., Noegel, A. A., Gotzmann, J., Foisner, R. and Karakesisoglou, I. (2005). The inner nuclear membrane protein Sun1 mediates the anchorage of Nesprin-2 to the nuclear envelope. *J. Cell Sci.* **118**, 3419-3430.
Penkner, A., Tang, L., Novatchkova, M., Ladurner, M., Fridkin, A., Gruenbaum, Y., Schweizer, D., Loidl, J. and Jantsch, V. (2007). The nuclear envelope protein Matefin/SUN-1 is required for homologous pairing in C. elegans meiosis. *Dev. Cell* **12**, 873-885.
Pickersgill, H., Kalverda, B., de W. E., Talhout, W., Fornerod, M. and van Steensel, B. (2006). Characterization of the Drosophila melanogaster genome at the nuclear lamina. *Nat. Genet.* **38**, 1005-1014.
Raff, J. W. (1999). The missing (L) UNC? *Curr. Biol.* **9,** R708-R710.
Reddy, K. L., Zullo, J. M., Bertolino, E. and Singh, H. (2008). Transcriptional repression mediated by repositioning of genes to the nuclear lamina. *Nature* **452**, 243-247.
Russell, L., Ettlin, R., Sinha, A. and Clegg, E. (1990). *Histological and Histopathological Evaluation of the Testis.* Clearwater, FL: Cache River Press.
Scherthan, H., Jerratsch, M., Li, B., Smith, S., Hulten, M., Lock, T. and de Lange, T. (2000). Mammalian meiotic telomeres: protein composition and redistribution in relation to nuclear pores. *Mol. Biol. Cell* **11**, 4189-4203.
Schirmer, E. C., Florens, L., Guan, T., Yates, J. R., 3rd and Gerace, L. (2003). Nuclear membrane proteins with potential disease links found by subtractive proteomics. *Science* **301**, 1380-1382.
Schneider, R. and Grosschedl, R. (2007). Dynamics and interplay of nuclear architecture, genome organization, and gene expression. *Genes Dev.* **21**, 3027-3043.
Sciurano, R., Rahn, M., Rey-Valzacchi, G. and Solari, A. J. (2007). The asynaptic chromatin in spermatocytes of translocation carriers contains the histone variant gamma-H2AX and associates with the XY body. *Hum. Reprod.* **22**, 142-150.
Seto, A. G., Kingston, R. E. and Lau, N. C. (2007). The coming of age for Piwi proteins. *Mol. Cell* **26**, 603-609.
Shaklai, S., Amariglio, N., Rechavi, G. and Simon, A. J. (2007). Gene silencing at the nuclear periphery. *FEBS J.* **274**, 1383-1392.
Stewart, C. L., Roux, K. J. and Burke, B. (2007). Blurring the boundary: the nuclear envelope extends its reach. *Science* **318**, 1408-1412.
Sullivan, T., Escalante-Alcalde, D., Bhatt, H., Anver, M., Bhat, N., Nagashima, K., Stewart, C. L. and Burke, B. (1999). Loss of A-type lamin expression compromises nuclear envelope integrity leading to muscular dystrophy. *J. Cell Biol.* **147**, 913-920.
Taddei, A., Van Houwe, G., Hediger, F., Kalck, V., Cubizolles, F., Schober, H. and Gasser, S. M. (2006). Nuclear pore association confers optimal expression levels for an inducible yeast gene. *Nature* **441**, 774-778.
Tanaka, S. S., Toyooka, Y., Akasu, R., Katoh-Fukui, Y., Nakahara, Y., Suzuki, R., Yokoyama, M. and Noce, T. (2000). The mouse homolog of Drosophila Vasa is required for the development of male germ cells. *Genes Dev.* **14**, 841-853.
Tomita, K. and Cooper, J. P. (2006). The meiotic chromosomal bouquet: SUN collects flowers. *Cell* **125**, 19-21.
Trinkle-Mulcahy, L. and Lamond, A. I. (2007). Toward a high-resolution view of nuclear dynamics. *Science* **318**, 1402-1407.
Viera, A., Santos, J. L., Page, J., Parra, M. T., Calvente, A., Cifuentes, M., Gomez, R., Lira, R., Suja, J. A. and Rufas, J. S. (2004). DNA double-strand breaks, recombination and synapsis: the timing of meiosis differs in grasshoppers and flies. *EMBO Rep.* **5**, 385-391.
Wagner, N. and Krohne, G. (2007). LEM-Domain proteins: new insights into lamin-interacting proteins. *Int. Rev. Cytol.* **261**, 1-46.
Worman, H. J. and Courvalin, J. C. (2004). How do mutations in lamins A and C cause disease? *J. Clin. Invest.* **113**, 349-351.
Zickler, D. (2006). From early homologue recognition to synaptonemal complex formation. *Chromosoma* **115**, 158-174.

Table S1. Expression (*Sun1*$^{-/-}$ versus *Sun1*$^{+/+}$) of housekeeping genes (Actin and Gapdh) and Sun1 by microarray

	P9 testis			P14 testis		MEFs	
Gene	Entrez Gene ID	Log_2 (*Sun1*$^{-/-}$/*wt*)	*P* value	Log_2 (Sun1$^{-/-}$/wt)	*P* value	Log_2 (*Sun1*$^{-/-}$/*wt*)	*P* value
Actb	11461	0.32	0.0652	0.86	0.0050	0.77	0.1562
Actb	11461	0.33	0.0654	0.86	0.0054	0.78	0.1800
Actb	11461	0.30	0.0754	0.82	0.0085	0.77	0.2208
Gapdh	14433	0.29	0.0724	0.36	0.0399	0.82	0.2316
Unc84A	77053	-2.60	0.00027	-3.14	0.00950	-1.99	0.0499

Data are presented in log2 scale.

Table S2. Differential expression of reproductive genes in P9 and P14 testes

P9 Reproductive genes

Gene	Log_2 (*Sun1*$^{-/-}$/*wt*)	*P* value	Entrez Gene ID	Description
Rnf17	-0.978	0.0054	30054	ring finger protein 17 (Rnf17), mRNA.
Aff4	-0.949	0.0478	93736	AF4/FMR2 family, member 4 (Aff4), mRNA.
Rnf17	-0.936	0.0005	30054	Ring finger protein 17
Ptgdr	-0.891	0.0357	19214	prostaglandin D receptor (Ptgdr), mRNA.
Adam3	-0.833	0.0041	11497	a disintegrin and metallopeptidase domain 3 (cyritestin) (Adam3), mRNA.
Plcd4	-0.752	0.0279	18802	phospholipase C, delta 4 (Plcd4), transcript variant 1, mRNA.
Psme4	-0.700	0.0217	103554	proteasome (prosome, macropain) activator subunit 4 (Psme4), mRNA.
Psg23	-0.696	0.0497	56868	pregnancy-specific glycoprotein 23 (Psg23), mRNA.
Prm2	-0.636	0.0357	19119	protamine 2 (Prm2), mRNA.
Nr2c2	-0.614	0.0037	22026	Nuclear receptor subfamily 2, group C, member 2
Npas3	-0.595	0.0307	27386	neuronal PAS domain protein 3 (Npas3), mRNA.
Tlk2	-0.588	0.0179	24086	tousled-like kinase 2 (Arabidopsis) (Tlk2), transcript variant B, mRNA.
Psg19	-0.565	0.0345	26439	Pregnancy specific glycoprotein 19
Zfp148	-0.565	0.0233	22661	zinc finger protein 148 (Zfp148), mRNA.
Aaas	-0.561	0.0370	223921	achalasia, adrenocortical insufficiency, alacrimia (Aaas), mRNA.
Foxl2	-0.548	0.0083	26927	forkhead box L2 (Foxl2), mRNA.
Dynll1	-0.535	0.0011	56455	Dynein light chain LC8-type 1
Creb1	-0.534	0.0164	12912	cAMP responsive element binding protein 1 (Creb1), transcript variant B, mRNA.
Mycbpap	-0.521	0.0237	104601	Mycbp associated protein
Pthlh	-0.502	0.0452	19227	Parathyroid hormone-like peptide
Odf2	-0.500	0.0084	18286	outer dense fiber of sperm tails 2 (Odf2), transcript variant 3, mRNA.
Pdgfra	-0.491	0.0306	18595	Platelet derived growth factor receptor, alpha polypeptide
Alms1	-0.466	0.0035	236266	Alstrom syndrome 1 homolog (human) (Alms1), mRNA.
Ddo	-0.457	0.0255	70503	D-aspartate oxidase (Ddo), mRNA.
Rnf17	-0.451	0.0078	30054	ring finger protein 17 (Rnf17), mRNA.
Kdr	-0.444	0.0149	16542	kinase insert domain protein receptor (Kdr), mRNA.
Zfp35	-0.423	0.0155	22694	zinc finger protein 35 (Zfp35), mRNA.
Plcd4	-0.411	0.0424	18802	Phospholipase C, delta 4
Tlk2	-0.409	0.0142	24086	tousled-like kinase 2 (Arabidopsis) (Tlk2), transcript variant B, mRNA.
Ccna1	-0.399	0.0420	12427	cyclin A1 (Ccna1), mRNA.
Tgfbr1	-0.389	0.0256	21812	Transforming growth factor, beta receptor I
Tgfbr1	-0.370	0.0054	21812	transforming growth factor, beta receptor I (Tgfbr1), mRNA.
Aplp2	-0.359	0.0165	11804	amyloid beta (A4) precursor-like protein 2 (Aplp2), transcript variant 3, mRNA.
Spag16	-0.353	0.0067	66722	sperm associated antigen 16 (Spag16), transcript variant 2, mRNA.
Ssty2	-0.302	0.0281	70009	spermiogenesis specific transcript on the Y 2 (Ssty2), mRNA.
A2m	-0.273	0.0492	232345	alpha-2-macroglobulin (A2m), mRNA.
Ift81	-0.269	0.0430	12589	intraflagellar transport 81 homolog (Chlamydomonas) (Ift81), mRNA.
Nos2	-0.261	0.0098	18126	nitric oxide synthase 2, inducible, macrophage (Nos2), mRNA.
Vegfa	-0.253	0.0125	22339	vascular endothelial growth factor A (Vegfa), transcript variant 5, mRNA.
Dnaja1	-0.227	0.0268	15502	DnaJ (Hsp40) homolog, subfamily A, member 1 (Dnaja1), mRNA.
Calca	-0.205	0.0485	12310	calcitonin/calcitonin-related polypeptide, alpha (Calca), transcript variant 1, mRNA.
Golga3	-0.177	0.0156	269682	golgi autoantigen, golgin subfamily a, 3 (Golga3), mRNA.
Prm3	-0.175	0.0388	19120	protamine 3 (Prm3), mRNA.
Nr2c2	-0.175	0.0212	22026	Nuclear receptor subfamily 2, group C, member 2
Atp8b3	-0.148	0.0377	67331	ATPase, class I, type 8B, member 3 (Atp8b3), mRNA.
Mbd2	-0.138	0.0403	17191	Methyl-CpG binding domain protein 2
Fgf9	-0.058	0.0324	14180	fibroblast growth factor 9 (Fgf9), mRNA.
Herpud2	0.145	0.0108	80517	HERPUD family member 2 (Herpud2), mRNA.
Hsd17b4	0.163	0.0092	15488	hydroxysteroid (17-beta) dehydrogenase 4 (Hsd17b4), mRNA.
Gnpda1	0.190	0.0103	26384	glucosamine-6-phosphate deaminase 1 (Gnpda1), mRNA.
Hexa	0.208	0.0064	15211	hexosaminidase A (Hexa), mRNA.
Ppp1r1b	0.209	0.0239	19049	protein phosphatase 1, regulatory (inhibitor) subunit 1B (Ppp1r1b), mRNA.
Tial1	0.214	0.0106	21843	Tia1 cytotoxic granule-associated RNA binding protein-like 1 (Tial1), mRNA.
Pafah1b2	0.223	0.0351	18475	platelet-activating factor acetylhydrolase, isoform 1b, alpha2 subunit (Pafah1b2), mRNA.
Fancg	0.233	0.0316	60534	Fanconi anemia, complementation group G (Fancg), mRNA.
Crtap	0.243	0.0239	56693	cartilage associated protein (Crtap), mRNA.
Brd2	0.244	0.0197	14312	bromodomain containing 2 (Brd2), transcript variant 1, mRNA.
Pbx1	0.246	0.0442	18514	pre B-cell leukemia transcription factor 1 (Pbx1), transcript variant b, mRNA.
Cugbp1	0.257	0.0139	13046	CUG triplet repeat, RNA binding protein 1 (Cugbp1), transcript variant 2, mRNA.
Grn	0.273	0.0099	14824	granulin (Grn), mRNA.
Asb1	0.275	0.0376	65247	ankyrin repeat and SOCS box-containing protein 1 (Asb1), transcript variant 1, mRNA.
Akt1	0.275	0.0311	11651	thymoma viral proto-oncogene 1 (Akt1), mRNA.
Bmp8a	0.284	0.0397	12163	bone morphogenetic protein 8a (Bmp8a), mRNA.

Ehmt2	0.288	0.0307	110147	euchromatic histone lysine N-methyltransferase 2 (Ehmt2), transcript variant short, mRNA.
Hsf1	0.290	0.0169	15499	heat shock factor 1 (Hsf1), mRNA.
Fcgbp	0.291	0.0266	215384	Fc fragment of IgG binding protein
Vegfa	0.307	0.0405	22339	Vascular endothelial growth factor A
Akt1	0.336	0.0372	11651	Thymoma viral proto-oncogene 1
Spata9	0.340	0.0042	75571	Spermatogenesis associated 9
Tssk6	0.355	0.0344	83984	testis-specific serine kinase 6 (Tssk6), mRNA.
Usf2	0.365	0.0245	22282	upstream transcription factor 2 (Usf2), mRNA.
Bcl2l2	0.376	0.0281	12050	Bcl2-like 2
Siah1a	0.390	0.0291	20437	seven in absentia 1A (Siah1a), mRNA.
Klf9	0.393	0.0245	16601	Kruppel-like factor 9 (Klf9), mRNA.
Bmp4	0.403	0.0117	12159	bone morphogenetic protein 4 (Bmp4), mRNA.
Fancc	0.406	0.0286	14088	Fanconi anemia, complementation group C (Fancc), transcript variant 2, mRNA.
Dazap1	0.408	0.0215	70248	DAZ associated protein 1 (Dazap1), transcript variant 1, mRNA.
Smcp	0.412	0.0109	17235	sperm mitochondria-associated cysteine-rich protein (Smcp), nuclear gene encoding mitochondrial protein, mRNA.
Nr0b1	0.422	0.0262	11614	nuclear receptor subfamily 0, group B, member 1 (Nr0b1), mRNA.
Nr5a1	0.424	0.0291	26423	nuclear receptor subfamily 5, group A, member 1 (Nr5a1), mRNA.
Dynll1	0.428	0.0097	56455	dynein light chain LC8-type 1 (Dynll1), mRNA.
S100a11	0.433	0.0043	20195	S100 calcium binding protein A11 (calgizzarin) (S100a11), mRNA.
Ercc1	0.435	0.0069	13870	excision repair cross-complementing rodent repair deficiency, complementation group 1 (Ercc1), mRNA.
Nr6a1	0.437	0.0143	14536	nuclear receptor subfamily 6, group A, member 1 (Nr6a1), mRNA.
Pebp1	0.440	0.0044	23980	phosphatidylethanolamine binding protein 1 (Pebp1), mRNA.
Ube2b	0.444	0.0319	22210	Ubiquitin-conjugating enzyme E2B, RAD6 homology (S. cerevisiae)
Cldn11	0.451	0.0011	18417	claudin 11 (Cldn11), mRNA.
Btg1	0.464	0.0424	12226	B-cell translocation gene 1, anti-proliferative (Btg1), mRNA.
Dazap1	0.467	0.0024	70248	DAZ associated protein 1
Pebp1	0.467	0.0029	23980	Phosphatidylethanolamine binding protein 1
Bmp4	0.470	0.0017	12159	bone morphogenetic protein 4 (Bmp4), mRNA.
Amhr2	0.513	0.0039	110542	anti-Mullerian hormone type 2 receptor (Amhr2), mRNA.
Adam25	0.526	0.0084	23793	a disintegrin and metallopeptidase domain 25 (testase 2) (Adam25), mRNA.
Insl3	0.527	0.0331	16336	insulin-like 3 (Insl3), mRNA.
Tcf21	0.529	0.0379	21412	transcription factor 21 (Tcf21), mRNA.
S100a11	0.549	0.0208	20195	S100 calcium binding protein A11 (calgizzarin)
Tcf7l2	0.557	0.0267	21416	Transcription factor 7-like 2, T-cell specific, HMG-box
Gtrgeo22	0.594	0.0066	110012	gene trap ROSA b-geo 22 (Gtrgeo22), mRNA.
H2afx	0.599	0.0008	15270	H2A histone family, member X (H2afx), mRNA.
Gpx4	0.607	0.0242	625249	glutathione peroxidase 4 (Gpx4), transcript variant 2, mRNA.
Bcl2l2	0.607	0.0222	12050	Bcl2-like 2 (Bcl2l2), mRNA.
Nhp2l1	0.608	0.0173	20826	NHP2 non-histone chromosome protein 2-like 1 (S. cerevisiae)
Cugbp1	0.625	0.0090	13046	CUG triplet repeat, RNA binding protein 1
Ybx2	0.633	0.0388	53422	Y box protein 2 (Ybx2), mRNA.
Sox3	0.635	0.0401	20675	SRY-box containing gene 3 (Sox3), mRNA.
Qk	0.644	0.0079	19317	Similar to quaking type II
Gamt	0.653	0.0078	14431	guanidinoacetate methyltransferase (Gamt), mRNA.
Gli1	0.655	0.0004	14632	GLI-Kruppel family member GLI1 (Gli1), mRNA.
B4galt1	0.660	0.0164	14595	UDP-Gal:betaGlcNAc beta 1,4- galactosyltransferase, polypeptide 1 (B4galt1), mRNA.
Ggnbp1	0.672	0.0217	70772	Gametogenetin binding protein 1
Magohb	0.689	0.0078	66441	mago-nashi homolog B (Drosophila) (Magohb), mRNA.
Magoh	0.726	0.0114	17149	mago-nashi homolog, proliferation-associated (Drosophila) (Magoh), mRNA.
Nme1	0.728	0.0089	18102	non-metastatic cells 1, protein (NM23A) expressed in (Nme1), mRNA.
Tssk2	0.794	0.0353	22115	testis-specific serine kinase 2 (Tssk2), mRNA.
Pafah1b1	0.812	0.0008	18472	platelet-activating factor acetylhydrolase, isoform 1b, beta1 subunit (Pafah1b1), mRNA.
Banf1	0.844	0.0038	23825	barrier to autointegration factor 1 (Banf1), transcript variant 1, mRNA.
Pafah1b1	0.854	0.0008	18472	platelet-activating factor acetylhydrolase, isoform 1b, beta1 subunit (Pafah1b1), mRNA.
Spo11	2.493	0.0249	26972	sporulation protein, meiosis-specific, SPO11 homolog (S. cerevisiae) (Spo11), transcript variant 2, mRNA.
Cit	3.436	0.0028	12704	citron (Cit), mRNA.

P14 reproductive genes

Gene	Log_2 (*Sun1*$^{-/-}$/*wt*)	*P* value	Entrez Gene ID	Description
Gykl1	-4.611	0.0005	14625	glycerol kinase-like 1 (Gykl1), mRNA.
Acr	-3.999	0.0130	11434	preproacrosin (Acr), mRNA.
Spag6	-3.748	0.0045	50525	sperm associated antigen 6 (Spag6), mRNA.
Odf4	-3.474	0.0045	252868	outer dense fiber of sperm tails 4 (Odf4), mRNA.
Piwil1	-3.316	0.0035	57749	piwi-like homolog 1 (Drosophila) (Piwil1), mRNA.
Adam3	-3.226	0.0164	11497	a disintegrin and metallopeptidase domain 3 (cyritestin) (Adam3), mRNA.
Spag16	-2.802	0.0086	66722	sperm associated antigen 16 (Spag16), transcript variant 2, mRNA.
Tcp11	-2.774	0.0079	21463	t-complex protein 11 (Tcp11), transcript variant 2, mRNA.
Clgn	-2.469	0.0030	12745	calmegin (Clgn), mRNA.
Atp8b3	-2.396	0.0065	67331	ATPase, class I, type 8B, member 3 (Atp8b3), mRNA.
Clgn	-2.379	0.0022	12745	Calmegin
4932415G16Rik	-2.293	0.0057	271036	RIKEN cDNA 4932415G16 gene (4932415G16Rik), mRNA.
Spag16	-2.266	0.0066	66722	sperm associated antigen 16 (Spag16), transcript variant 2, mRNA.
Atp8b3	-2.024	0.0361	67331	ATPase, class I, type 8B, member 3
Ybx2	-1.864	0.0028	53422	Y box protein 2 (Ybx2), mRNA.
Mtl5	-1.420	0.0195	17771	metallothionein-like 5, testis-specific (tesmin) (Mtl5), transcript variant 1, mRNA.
Zpbp2	-1.408	0.0183	69376	zona pellucida binding protein 2 (Zpbp2), transcript variant 2, mRNA.
Nme5	-1.283	0.0208	75533	expressed in non-metastatic cells 5 (Nme5), mRNA.
Tnp2	-1.230	0.0007	21959	transition protein 2 (Tnp2), mRNA.
Aff4	-1.219	0.0017	93736	AF4/FMR2 family, member 4 (Aff4), mRNA.
Rnf17	-1.171	0.0145	30054	Ring finger protein 17
Ubr2	-1.168	0.0077	224826	ubiquitin protein ligase E3 component n-recognin 2 (Ubr2), mRNA.
Crem	-1.155	0.0067	12916	CAMP responsive element modulator
Msh4	-1.152	0.0119	55993	mutS homolog 4 (E. coli) (Msh4), mRNA.
Odf2	-1.121	0.0123	18286	outer dense fiber of sperm tails 2 (Odf2), mRNA.
Crem	-1.110	0.0222	12916	CAMP responsive element modulator
Spa17	-1.045	0.0045	20686	sperm autoantigenic protein 17 (Spa17), mRNA.
Aaas	-1.044	0.0238	223921	achalasia, adrenocortical insufficiency, alacrimia (Aaas), mRNA.
Rnf17	-1.035	0.0397	30054	ring finger protein 17 (Rnf17), mRNA.
D1Pas1	-0.970	0.0241	110957	DNA segment, Chr 1, Pasteur Institute 1 (D1Pas1), mRNA.
Spin4	-0.956	0.0174	270624	spindlin family, member 4 (Spin4), mRNA.
Nr2c2	-0.955	0.0242	22026	nuclear receptor subfamily 2, group C, member 2 (Nr2c2), mRNA.
Dmrtc2	-0.936	0.0068	71241	doublesex and mab-3 related transcription factor like family C2 (Dmrtc2), mRNA.
Zscan2	-0.921	0.0156	22691	zinc finger and SCAN domain containing 2 (Zscan2), mRNA.
Mycbpap	-0.909	0.0043	104601	Mycbp associated protein (Mycbpap), mRNA.
Boll	-0.878	0.0222	75388	Bol, boule-like (Drosophila)
Boll	-0.874	0.0157	75388	bol, boule-like (Drosophila) (Boll), mRNA.
Ddx25	-0.801	0.0136	30959	DEAD (Asp-Glu-Ala-Asp) box polypeptide 25 (Ddx25), mRNA.
Fancd2	-0.800	0.0046	211651	Fanconi anemia, complementation group D2 (Fancd2), mRNA.
Zfp35	-0.793	0.0043	22694	zinc finger protein 35 (Zfp35), mRNA.
Tlk2	-0.786	0.0091	24086	tousled-like kinase 2 (Arabidopsis) (Tlk2), mRNA.
Morc1	-0.774	0.0153	17450	microrchidia 1 (Morc1), mRNA.
Zpbp	-0.744	0.0183	53604	zona pellucida binding protein (Zpbp), mRNA.
Hook1	-0.704	0.0221	77963	hook homolog 1 (Drosophila) (Hook1), mRNA.
Strbp	-0.688	0.0121	20744	spermatid perinuclear RNA binding protein (Strbp), mRNA.
Spo11	-0.688	0.0071	26972	sporulation protein, meiosis-specific, SPO11 homolog (S. cerevisiae) (Spo11), transcript variant 1, mRNA.
Adad1	-0.663	0.0163	21744	adenosine deaminase domain containing 1 (testis specific) (Adad1), mRNA.
Tlk2	-0.652	0.0048	24086	tousled-like kinase 2 (Arabidopsis) (Tlk2), mRNA.
Dzip1	-0.649	0.0227	66573	DAZ interacting protein 1 (Dzip1), mRNA.
Chd7	-0.627	0.0113	320790	chromodomain helicase DNA binding protein 7 (Chd7), mRNA.
Spag1	-0.595	0.0180	26942	sperm associated antigen 1 (Spag1), mRNA.
Pcyt1b	-0.569	0.0421	236899	phosphate cytidylyltransferase 1, choline, beta isoform (Pcyt1b), transcript variant 2, mRNA.
Chd7	-0.557	0.0185	320790	chromodomain helicase DNA binding protein 7 (Chd7), mRNA.
Rnf17	-0.534	0.0387	30054	ring finger protein 17 (Rnf17), mRNA.
Creb1	-0.519	0.0144	12912	cAMP responsive element binding protein 1 (Creb1), transcript variant C, mRNA.
Gmcl1	-0.518	0.0265	23885	germ cell-less homolog 1 (Drosophila) (Gmcl1), mRNA.
Lgr4	-0.509	0.0139	107515	leucine-rich repeat-containing G protein-coupled receptor 4 (Lgr4), mRNA.
Styx	-0.508	0.0394	56291	phosphoserine/threonine/tyrosine interaction protein (Styx), mRNA.
Spata6	-0.459	0.0200	67946	spermatogenesis associated 6 (Spata6), mRNA.
Ift81	-0.454	0.0471	12589	intraflagellar transport 81 homolog (Chlamydomonas) (Ift81), mRNA.
H1fnt	-0.433	0.0142	70069	H1 histone family, member N, testis-specific (H1fnt), mRNA.
Zfp148	-0.406	0.0033	22661	zinc finger protein 148 (Zfp148), mRNA.
Tubd1	-0.403	0.0261	56427	tubulin, delta 1 (Tubd1), mRNA.

Strbp	-0.385	0.0175	20744	spermatid perinuclear RNA binding protein (Strbp), mRNA.
Golga3	-0.383	0.0378	269682	golgi autoantigen, golgin subfamily a, 3 (Golga3), mRNA.
Psg19	-0.382	0.0459	26439	pregnancy specific glycoprotein 19 (Psg19), mRNA.
Ddx1	-0.370	0.0070	104721	DEAD (Asp-Glu-Ala-Asp) box polypeptide 1 (Ddx1), mRNA.
Creb1	-0.368	0.0091	12912	cAMP responsive element binding protein 1 (Creb1), transcript variant B, mRNA.
Zfp41	-0.343	0.0159	22701	zinc finger protein 41 (Zfp41), transcript variant 2, mRNA.
Sbf1	-0.323	0.0183	77980	SET binding factor 1 (Sbf1), mRNA.
Rps6kb1	-0.318	0.0386	72508	ribosomal protein S6 kinase, polypeptide 1 (Rps6kb1), mRNA.
Kdr	-0.302	0.0404	16542	kinase insert domain protein receptor (Kdr), mRNA.
Tcf7l2	-0.296	0.0142	21416	Transcription factor 7-like 2, T-cell specific, HMG-box
Hrb	-0.290	0.0103	15463	HIV-1 Rev binding protein
Tbpl1	-0.285	0.0362	237336	TATA box binding protein-like 1 (Tbpl1), mRNA.
Bmpr1a	-0.266	0.0370	12166	bone morphogenetic protein receptor, type 1A (Bmpr1a), mRNA.
Dnaja1	-0.186	0.0357	15502	DnaJ (Hsp40) homolog, subfamily A, member 1 (Dnaja1), mRNA.
Cdc25b	-0.179	0.0237	12531	Cell division cycle 25 homolog B (S. pombe)
Mlh1	-0.152	0.0219	17350	mutL homolog 1 (E. coli) (Mlh1), mRNA.
Diap2	-0.117	0.0273	54004	Diaphanous homolog 2 (Drosophila)
Spata6	-0.040	0.0168	67946	Spermatogenesis associated 6
Acox1	0.063	0.0210	11430	acyl-Coenzyme A oxidase 1, palmitoyl (Acox1), mRNA.
Nr2c2	0.116	0.0340	22026	Nuclear receptor subfamily 2, group C, member 2
Spata20	0.148	0.0465	217116	spermatogenesis associated 20 (Spata20), mRNA.
Ercc1	0.166	0.0304	13870	excision repair cross-complementing rodent repair deficiency, complementation group 1 (Ercc1), mRNA.
Siah1a	0.171	0.0302	20437	seven in absentia 1A (Siah1a), mRNA.
Sox9	0.192	0.0361	20682	SRY-box containing gene 9 (Sox9), mRNA.
Nr0b1	0.199	0.0257	11614	nuclear receptor subfamily 0, group B, member 1 (Nr0b1), mRNA.
Fkbp4	0.206	0.0255	14228	FK506 binding protein 4 (Fkbp4), mRNA.
Tcf7l2	0.217	0.0264	21416	Transcription factor 7-like 2, T-cell specific, HMG-box
Tgfb1	0.230	0.0381	21803	transforming growth factor, beta 1 (Tgfb1), mRNA.
Tcf7l2	0.240	0.0429	21416	transcription factor 7-like 2, T-cell specific, HMG-box (Tcf7l2), mRNA.
Cetn2	0.257	0.0413	26370	centrin 2 (Cetn2), mRNA.
Crem	0.268	0.0292	12916	cAMP responsive element modulator (Crem), mRNA.
P42pop	0.271	0.0140	232934	Myb protein P42POP (P42pop), mRNA.
Dhcr24	0.282	0.0104	74754	24-dehydrocholesterol reductase (Dhcr24), mRNA.
Dnd1	0.283	0.0082	213236	dead end homolog 1 (zebrafish) (Dnd1), mRNA.
Cit	0.287	0.0054	12704	Citron
Tial1	0.305	0.0377	21843	Tia1 cytotoxic granule-associated RNA binding protein-like 1 (Tial1), mRNA.
Zfp148	0.310	0.0162	22661	zinc finger protein 148 (Zfp148), mRNA.
Cdc25b	0.312	0.0030	12531	Cell division cycle 25 homolog B (S. pombe)
Nkd1	0.317	0.0065	93960	naked cuticle 1 homolog (Drosophila) (Nkd1), mRNA.
Hrb	0.320	0.0202	15463	HIV-1 Rev binding protein
Dmrt3	0.333	0.0093	240590	doublesex and mab-3 related transcription factor 3 (Dmrt3), mRNA.
Sox9	0.334	0.0017	20682	SRY-box containing gene 9 (Sox9), mRNA.
Brd2	0.340	0.0140	14312	bromodomain containing 2 (Brd2), transcript variant 1, mRNA.
Crtap	0.342	0.0223	56693	cartilage associated protein (Crtap), mRNA.
Rhox5	0.346	0.0028	18617	reproductive homeobox 5 (Rhox5), mRNA.
Cugbp1	0.350	0.0187	13046	CUG triplet repeat, RNA binding protein 1
Rhox5	0.353	0.0296	18617	reproductive homeobox 5 (Rhox5), mRNA.
Gpx4	0.355	0.0253	625249	glutathione peroxidase 4 (Gpx4), transcript variant 2, mRNA.
Hexb	0.365	0.0293	15212	hexosaminidase B (Hexb), mRNA.
Sox3	0.380	0.0197	20675	SRY-box containing gene 3 (Sox3), mRNA.
Gli1	0.386	0.0391	14632	GLI-Kruppel family member GLI1 (Gli1), mRNA.
Nanog	0.387	0.0159	71950	Nanog homeobox
Figla	0.400	0.0037	26910	folliculogenesis specific basic helix-loop-helix (Figla), mRNA.
Gtrgeo22	0.405	0.0142	110012	gene trap ROSA b-geo 22 (Gtrgeo22), mRNA.
Dynll1	0.413	0.0083	56455	dynein light chain LC8-type 1 (Dynll1), mRNA.
2010012 C16Rik	0.419	0.0089	66441	RIKEN cDNA 2010012C16 gene (2010012C16Rik), mRNA.
Magoh	0.430	0.0205	17149	mago-nashi homolog, proliferation-associated (Drosophila) (Magoh), mRNA.
Usf2	0.431	0.0019	22282	upstream transcription factor 2 (Usf2), mRNA.
Adamts2	0.432	0.0363	216725	A disintegrin-like and metallopeptidase (reprolysin type) with thrombospondin type 1 motif, 2
Btg1	0.441	0.0093	12226	B-cell translocation gene 1, anti-proliferative (Btg1), mRNA.
Pthlh	0.443	0.0321	19227	Parathyroid hormone-like peptide
Nr5a1	0.448	0.0017	26423	nuclear receptor subfamily 5, group A, member 1 (Nr5a1), mRNA.
Pafah1b3	0.454	0.0016	18476	platelet-activating factor acetylhydrolase, isoform 1b, alpha1 subunit (Pafah1b3), mRNA.
Pebp1	0.461	0.0310	23980	phosphatidylethanolamine binding protein 1 (Pebp1), mRNA.
Nhp2l1	0.465	0.0045	20826	NHP2 non-histone chromosome protein 2-like 1 (S. cerevisiae)
Amhr2	0.472	0.0230	110542	anti-Mullerian hormone type 2 receptor (Amhr2), mRNA.

Stat3	0.474	0.0238	20848	signal transducer and activator of transcription 3 (Stat3), transcript variant 3, mRNA.
Grn	0.475	0.0322	14824	granulin (Grn), mRNA.
Bcl2l2	0.478	0.0009	12050	Bcl2-like 2 (Bcl2l2), mRNA.
Rps6ka2	0.484	0.0166	20112	ribosomal protein S6 kinase, polypeptide 2 (Rps6ka2), mRNA.
Spin1	0.486	0.0246	20729	spindlin 1 (Spin1), transcript variant 1, mRNA.
Akt1	0.488	0.0145	11651	thymoma viral proto-oncogene 1 (Akt1), mRNA.
Ehmt2	0.492	0.0268	110147	euchromatic histone lysine N-methyltransferase 2 (Ehmt2), transcript variant short, mRNA.
Akt1	0.493	0.0003	11651	Thymoma viral proto-oncogene 1
Sohlh1	0.507	0.0282	227631	spermatogenesis and oogenesis specific basic helix-loop-helix 1 (Sohlh1), mRNA.
Foxo3a	0.508	0.0384	56484	Forkhead box O3a
Bcap31	0.514	0.0145	27061	B-cell receptor-associated protein 31 (Bcap31), mRNA.
Cxcl12	0.526	0.0106	20315	chemokine (C-X-C motif) ligand 12 (Cxcl12), transcript variant 1, mRNA.
Nme1	0.530	0.0056	18102	expressed in non-metastatic cells 1, protein (Nme1), mRNA.
Cldn11	0.531	0.0213	18417	claudin 11 (Cldn11), mRNA.
Insl3	0.532	0.0019	16336	insulin-like 3 (Insl3), mRNA.
Nanos3	0.549	0.0281	244551	nanos homolog 3 (Drosophila) (Nanos3), mRNA.
Sod1	0.555	0.0156	20655	superoxide dismutase 1, soluble (Sod1), mRNA.
Nanos2	0.571	0.0408	378430	nanos homolog 2 (Drosophila) (Nanos2), mRNA.
S100a11	0.572	0.0240	20195	S100 calcium binding protein A11 (calgizzarin)
S100a11	0.575	0.0474	20195	S100 calcium binding protein A11 (calgizzarin) (S100a11), mRNA.
Vmo1	0.583	0.0111	327956	vitelline membrane outer layer 1 homolog (chicken) (Vmo1), mRNA.
Rgs2	0.587	0.0157	19735	regulator of G-protein signaling 2 (Rgs2), mRNA.
Bax	0.596	0.0036	12028	Bcl2-associated X protein (Bax), mRNA.
Gamt	0.607	0.0052	14431	guanidinoacetate methyltransferase (Gamt), mRNA.
Cd9	0.611	0.0491	12527	CD9 antigen (Cd9), mRNA.
Banf1	0.624	0.0024	23825	barrier to autointegration factor 1 (Banf1), transcript variant 1, mRNA.
Pafah1b1	0.648	0.0042	18472	platelet-activating factor acetylhydrolase, isoform 1b, beta1 subunit (Pafah1b1), mRNA.
Pafah1b1	0.677	0.0106	18472	platelet-activating factor acetylhydrolase, isoform 1b, beta1 subunit (Pafah1b1), mRNA.
Adam25	0.685	0.0028	23793	a disintegrin and metallopeptidase domain 25 (testase 2) (Adam25), mRNA.
Cxcl12	0.704	0.0159	20315	chemokine (C-X-C motif) ligand 12 (Cxcl12), transcript variant 2, mRNA.
Sod1	0.800	0.0144	20655	superoxide dismutase 1, soluble (Sod1), mRNA.
Klf9	0.972	0.0471	16601	Kruppel-like factor 9 (Klf9), mRNA.
Nr2c2	1.291	0.0019	22026	Nuclear receptor subfamily 2, group C, member 2